

**ISTANBUL TECHNICAL UNIVERSITY ★ GRADUATE SCHOOL OF SCIENCE**  
**ENGINEERING AND TECHNOLOGY**

**DESIGN OF DIFFERENTIAL TRANSIMPEDANCE AMPLIFIER  
IN SiGe BiCMOS FOR 10 Gbit/s FIBER OPTICAL RECEIVERS**

**M.Sc. THESIS**

**Yunus AKBAY  
(504061235)**

**Department of Electronics and Communication Engineering**

**Electronics Engineering Programme**

**Thesis Advisor: Prof. Dr. Osman PALAMUTÇUOĞULLARI**

**JANUARY 2014**



**İSTANBUL TEKNİK ÜNİVERSİTESİ ★ FEN BİLİMLERİ ENSTİTÜSÜ**

**10 Gbit/s FİBER OPTİK ALICILAR İÇİN SiGe BiCMOS  
FARKSAL GEÇİŞ-EMPEDANSI KUVVETLENDİRİCİSİ TASARIMI**

**YÜKSEK LİSANS TEZİ**

**Yunus AKBEY  
(504061235)**

**Elektronik ve Haberleşme Mühendisliği Anabilim dalı**

**Elektronik Mühendisliği Programı**

**Tez Danışmanı: Prof. Dr. Osman PALAMUTÇUOĞULLARI**

**OCAK 2014**



**Yunus Akbey**, a **M.Sc.** student of **ITU Graduate School of Science, Engineering and Technology**, student ID **504061235**, successfully defended the **thesis** entitled “**Design of Differential Transimpedance Amplifier in SiGe BiCMOS For 10 Gbit/s Fiber Optical Receivers**”, which he prepared after fulfilling the requirements specified in the associated legislations, before the jury whose signatures are below.

**Thesis Advisor :**      **Prof. Dr. Osman PALAMUTÇUOĞULRI**      .....

İstanbul Technical University

**Jury Members :**      **Prof. Dr. Selçuk Paker**      .....

İstanbul Technical University

**Prof. Dr. Burak Polat**      .....

Beykent University

**Date of Submission : 12 December 2013**

**Date of Defense : 24 January 2014**



*To my mother and father,*



## **FOREWORD**

I would like to express my sincere appreciations to my supervisor Prof. Dr. Osman PALAMUTÇUOĞULLARI. Without his vision, encouragements and feedback, this dissertation would never become a reality.

My biggest gratitude goes to my mother and father for being with me and supporting me at every moment of my life. In this point, I want to open a page for my mother. She always supported me during my entire education life. She always tried to do her best to give me a big support during the preparation of this thesis.

My deepest gratitude goes to my sister and my brothers; Yeliz AKBEY, Ferit AKBEY and Emrah AKBEY. They have always been with me when I make an important decision/action in my life. They have generously given financial and spiritual supports whenever I need.

December 2013

Yunus AKBEY



## TABLE OF CONTENTS

	<u>Page</u>
<b>FOREWORD</b> .....	<b>ix</b>
<b>TABLE OF CONTENTS</b> .....	<b>xi</b>
<b>ABBREVIATIONS</b> .....	<b>xiii</b>
<b>SYMBOLS</b> .....	<b>xv</b>
<b>LIST OF TABLES</b> .....	<b>xvii</b>
<b>LIST OF FIGURES</b> .....	<b>xix</b>
<b>SUMMARY</b> .....	<b>xxi</b>
<b>ÖZET</b> .....	<b>xxiii</b>
<b>1. INTRODUCTION</b> .....	<b>1</b>
1.1 Purpose of the Thesis .....	<b>2</b>
1.2 Thesis Outline.....	<b>3</b>
<b>2. FIBER OPTICAL COMMUNICATION SYSTEM</b> .....	<b>5</b>
2.1 Fiber Optic .....	<b>8</b>
2.2 Photodiode.....	<b>10</b>
<b>3. BACKGROUND, THEORY AND DESIGN CONSIDERATIONS</b> .....	<b>13</b>
3.1 Design Requirements .....	<b>14</b>
3.1.1 Sensitivity and bit-error-rate .....	<b>15</b>
3.1.2 Bandwidth considerations and ISI .....	<b>19</b>
3.2 Transimpedance Amplifier Design .....	<b>22</b>
3.2.1 Transimpedance amplifier specifications .....	<b>23</b>
3.2.1.1 Transimpedance .....	<b>23</b>
3.2.1.2 Bandwidth and group delay .....	<b>23</b>
3.2.1.3 Noise.....	<b>24</b>
3.2.1.4 Wide input dynamic range .....	<b>25</b>
3.2.1.5 Output impedance.....	<b>26</b>
3.2.2 TIA circuits concepts .....	<b>26</b>
3.2.2.1 Open-loop TIA.....	<b>28</b>
3.2.2.2 Feedback TIA.....	<b>29</b>
3.2.2.3 Differential TIA .....	<b>35</b>
3.3 Silicon-Germanium Heterojunction Transistors .....	<b>36</b>
<b>4. DESIGN OF DIFFERENTIAL TRANSIMPEDANCE AMPLIFIER in SiGe BiCMOS FOR 10 Gbit/s FIBER OPTICAL RECEIVERS</b> .....	<b>39</b>
4.1 Circuit Design .....	<b>39</b>
4.2 Simulation Results .....	<b>46</b>
<b>5. CONCLUSION</b> .....	<b>53</b>
<b>REFERENCES</b> .....	<b>55</b>
<b>APPENDICES</b> .....	<b>59</b>
<b>CURRICULUM VITAE</b> .....	<b>65</b>



## ABBREVIATIONS

<b>ac</b>	: Alternating Current
<b>AGC</b>	: Automatic Gain Control
<b>AMS</b>	: Austria Micro Systems
<b>AlGaAs</b>	: Aluminum Gallium Arsenide
<b>BER</b>	: Bit-Error-Rate
<b>BiCMOS</b>	: Bipolar Complementary Metal Oxide Semiconductor
<b>BJT</b>	: Bipolar Junction Transistor
<b>BW</b>	: Bandwidth
<b>CD</b>	: Compact Disc
<b>CDR</b>	: Clock and Data Recovery
<b>CG</b>	: Common-Gate
<b>CMOS</b>	: Complementary Metal Oxide Semiconductor
<b>CMU</b>	: Clock Multiplication Unit
<b>dB</b>	: decibel
<b>dBm</b>	: decibelmili
<b>DC</b>	: Direct Current
<b>DMUX</b>	: Demultiplexer
<b>EMI</b>	: Electromagnetic Interference
<b>ELECO</b>	: Electrical and Electronics Engineering Conference
<b>erfc</b>	: Complementary Error Function
<b>FET</b>	: Field-Effect Transistor
<b>GaAs</b>	: Gallium Arsenide
<b>GaN</b>	: Gallium Nitride
<b>GB</b>	: Gigabyte
<b>Gb</b>	: Gigabit
<b>Gbit</b>	: Gigabit
<b>Ge</b>	: Germanium
<b>GSM</b>	: Global System for Mobile Communications
<b>HBT</b>	: Heterojunction Bipolar Transistor
<b>HEMT</b>	: High-Electron Mobility Transistor
<b>IC</b>	: Integrated Circuit
<b>InGaAs</b>	: Indium Gallium Arsenide
<b>InP</b>	: Indium Phosphate
<b>ISI</b>	: Intersymbol Interference
<b>ISSCC</b>	: International Solid-State Circuits Conference
<b>LA</b>	: Limiting Amplifier
<b>LAN</b>	: Local Area Network
<b>LD</b>	: Laser Diode
<b>MESFET</b>	: Metal-Semiconductor Field-Effect Transistor
<b>MOS</b>	: Metal Oxide Semiconductor
<b>MUX</b>	: Multiplexer
<b>NRZ</b>	: Non-Return-to-Zero
<b>PA</b>	: Post Amplifier
<b>PD</b>	: Photodiode
<b>PIN</b>	: p-intrinsic-n
<b>prbs</b>	: Pseudorandom Bit Sequence

<b>P.M.</b>	: Phase Margin
<b>PO</b>	: Percent Overshoot
<b>pp</b>	: peak-to-peak
<b>rms</b>	: root mean square
<b>RF</b>	: Radio Frequency
<b>RZ</b>	: Return-to-Zero
<b>SDH</b>	: Synchronous Digital Hierarchy
<b>Si</b>	: Silicon
<b>SiO<sub>2</sub></b>	: Silicon Dioxide
<b>SNR</b>	: Signal to Noise Ratio
<b>SONET</b>	: Synchronous Optical Network
<b>TIA</b>	: Transimpedance Amplifier
<b>USA</b>	: United States of America
<b>VA</b>	: Voltage Amplifier
<b>WDM</b>	: Wavelength-Division Multiplexing

## SYMBOLS

$A$	: voltage gain
$A_0$	: DC voltage gain
$B_R$	: bit rate
$c$	: speed of light in vacuum
$C_{cs}$	: collector-substrate capacitance
$C_{in}$	: input capacitance
$C_{next}$	: input capacitance of the next stage
$C_o$	: total output capacitance
$C_{out}$	: output capacitance
$C_P$	: photodiode junction capacitance
$C_T$	: total input capacitance
$C_{\mu}$	: collector-base junction capacitance
$C_{\pi}$	: collector-emitter capacitance
$f_{.3dB}$	: bandwidth of TIA
$f_T$	: unity-current gain frequency
$g_m$	: transconductance
$h$	: Planck's constant
$I_B$	: base current
$I_C$	: collector current
$i_{in}$	: small-signal input current
$i_{in,pp}$	: peak-to-peak input current
$I_{PD}$	: photodiode current
$i_{sen}^{pp}$	: electrical sensitivity
$\bar{i}_{in}$	: averaged input current
$i_{n,in}^2$	: input-referred current spectrum
$\bar{i}_{n,in,tot}$	: total input-referred noise current
$\bar{i}_{n,in,avg}$	: averaged input-referred noise current
$k$	: Boltzmann constant
$km$	: kilometer
$mm$	: millimeter
$nm$	: nanometer
$n^+$	: n-doped
$Q(x)$	: Q function
$q$	: electrical charge
$P$	: error probability
$\bar{P}$	: averaged optical power
$P_{sen}$	: optical sensitivity
$p^+$	: p-doped
$r_b$	: base resistance
$R_C$	: load resistor
$R_F$	: feedback resistor
$R_{out}$	: output resistance
$R_T$	: DC transimpedance gain
$s$	: second
$T$	: temperature in Kelvin
$T_b$	: bit period

$t$	: time
$v_{n,tot}$	: total integrated output noise
$v_o$	: small-signal output voltage
$v_{out}$	: small-signal output voltage
$v_{pp}$	: peak-to-peak value of the output signal
$v_{n,o}^2$	: output noise voltage spectrum
$V_{TH}$	: threshold voltage of the decision circuit
$ Z_{TIA}(f) $	: frequency-dependent transimpedance magnitude
$Z_T$	: transimpedance gain
$\zeta$	: dimensionless damping ratio of a second-order system
$\eta$	: quantum efficiency of a photodiode
$\theta(f)$	: frequency-dependent phase shift
$\lambda$	: wavelength of light
$\mu$	: mobility
$\Delta f$	: unity-frequency
$ \Delta\tau $	: group delay variation
$\mu m$	: micrometer
$\mu A_{pp}$	: peak-to-peak microampere
$\mathcal{R}$	: responsivity of a photodiode
$\tau$	: time constant
$\tau(\omega)$	: group delay
$\omega_n$	: natural pulsation of a second-order system
$\omega_{-3dB}$	: bandwidth of a system
$\Omega$	: ohm
$\beta$	: current gain

## LIST OF TABLES

	<u>Page</u>
<b>Table 2.1</b> : SONET/SDH hierarchy.....	6
<b>Table 2.2</b> : PIN Photodiode operating wavelengths.....	11
<b>Table 3.1</b> : BER and Q relationship.....	18
<b>Table 4.1</b> : Device values and transistor emitter sizes.....	45
<b>Table 4.2</b> : Transistor biasing points.....	45
<b>Table 5.1</b> : TIA performance summary and comparison some existing works .....	54



## LIST OF FIGURES

	<u>Page</u>
<b>Figure 1.1</b> : Illustration of fiber optic receiver.....	2
<b>Figure 1.2</b> : Transimpedance amplifier design .....	3
<b>Figure 2.1</b> : Fiber Optical Communication system.....	6
<b>Figure 2.2</b> : NRZ and RZ data modulation.....	8
<b>Figure 2.3</b> : Cross-section of fiber and fiber types .....	8
<b>Figure 2.4</b> : PIN Photodiode and approximate small-signal model .....	10
<b>Figure 3.1</b> : A typical fiber optical front-end with shunt-feedback TIA. ....	14
<b>Figure 3.2</b> : Relationship between signal, noise and bit-error rate.....	15
<b>Figure 3.3</b> : Bit error probability at the CDR. ....	16
<b>Figure 3.4</b> : Practical BER curve of a receiver.....	18
<b>Figure 3.5</b> : RC network for analyzing ISI (a) periodic square wave (b) random data .....	20
<b>Figure 3.6</b> : Bit rate versus bandwidth .....	21
<b>Figure 3.7</b> : Typical shunt-feedback TIA.....	22
<b>Figure 3.8</b> : Low and high impedance TIA.....	27
<b>Figure 3.9</b> : Typical open-loop TIA topology.....	28
<b>Figure 3.10</b> : Second-order feedback transimpedance amplifier with small-signal equivalent. ....	30
<b>Figure 3.11</b> : Noise contributions in feedback TIA.....	33
<b>Figure 3.12</b> : Photodiode capacitance, $C_p$ , effect on noise performance of TIA.....	35
<b>Figure 3.13</b> : Differential TIA with replicated capacitance.....	36
<b>Figure 3.14</b> : Cross-section of vertical NPN SiGe transistor.....	37
<b>Figure 4.1</b> : Result of low bandwidth on Bessel and Butterworth TIAs.....	40
<b>Figure 4.2</b> : Realized differential SiGe TIA schematic. ....	42
<b>Figure 4.3</b> : Half-circuit model of the differential SiGe TIA with photodiode small- signal model.....	43
<b>Figure 4.4</b> : Differential transimpedance gain of the TIA.....	46
<b>Figure 4.5</b> : Group delay variation of the frequency response over the bandwidth .	47
<b>Figure 4.6</b> : Total input-referred noise current spectrum of the differential TIA .....	47
<b>Figure 4.7 (a)</b> : Differential output waveform of the circuit. The input data stream is NRZ 10 Gbit/s $2^{31} - 1$ PRBS. Input current is $15 \mu A_{pp}$ .....	49
<b>Figure 4.7 (b)</b> : Differential output waveform of the proposed TIA. The input data stream is NRZ 10 Gbit/s $2^{31} - 1$ PRBS. Input current is $400 \mu A_{pp}$ ....	49
<b>Figure 4.8</b> : Single-ended $S_{22}$ parameter of the realized TIA. $30 \Omega$ resistors are added to the both output for $50 \Omega$ matching .....	50
<b>Figure 4.9 (a)</b> : Eye diagrams showing differential output at 10 Gbit/s $2^{31} - 1$ PRBS data stream. Input current is $15 \mu A_{pp}$ , both outputs are loaded with 100 fF capacitor.....	51
<b>Figure 4.9 (b)</b> : Eye diagrams showing differential output at 10 Gbit/s $2^{31} - 1$ PRBS data stream. Input current is $300 \mu A_{pp}$ , both outputs are loaded with 100 fF capacitor.....	51

**Figure 4.9 (c)** : Eye diagrams showing differential output at 10 Gbit/s  $2^{31} - 1$  PRBS data stream. Input current is  $15 \mu A_{pp}$ , both outputs are loaded with  $50 \Omega$  resistors.  $30 \Omega$  matching resistors are added to the both outputs. .... 52

**Figure 4.9 (d)** : Eye diagrams showing differential output at 10 Gbit/s  $2^{31} - 1$  PRBS data stream. Input current is  $300 \mu A_{pp}$ , both outputs are loaded with  $50 \Omega$  resistors.  $30 \Omega$  matching resistors are added to the both outputs. .... 52

**Figure A.1** : Program schematic of realized TIA ..... 61

**Figure A.2** : Simulation and values ..... 62

**Figure A.3** : Noise contribution of each device ..... 63

## **DESIGN OF DIFFERENTIAL TRANSIMPEDANCE AMPLIFIER IN SiGe BiCMOS FOR 10 Gbit/s FIBER OPTICAL RECEIVERS**

### **SUMMARY**

After the beginning of 70s that first low loss silica fiber was presented, fiber optic communication has dominated to the telecommunication field and data transportation including short-haul and long-haul networks. The main reason for that fiber optic communication offers relatively very large bandwidth. Furthermore, the transmission using light keeps superior advantages over the conventional electrical communications such as no cross-talk, immune to the EMI, easy implementation and endurance.

Because fiber theoretically has enormous bandwidth and huge data transport capacity, heterostructure and heterojunction transistors such as GaAs and InP have dominated to photoreceivers since they exhibit very good bandwidth and noise performance simultaneously. SiGe BiCMOS however has provided cost-effective alternative for the realization of photoreceivers because SiGe BiCMOS can combine entire receiver in a single die. While high-gain, low-noise and high speed capability of SiGe is assisted for the analog part, CMOS circuits can build digital architecture of the optical receiver.

As for the receiver, the light transmitted by laser diode travels through fiber and experiences loss and dispersion before reaching a photodiode at the far end. The photodiode then senses the power of light and transforms the light intensity to a proportional photocurrent. At the receiver front-end, transimpedance amplifier (TIA) is an interface that converts the receiving photocurrent to electrical voltage. This amplified voltage generally is not enough for further digital processing. A second amplifier, namely post amplifier (PA), further increases the signal level. Clock and data recovery (CDR) extracts the digital data and clock information from the received signal. This is done by defining the threshold voltage. The pulse is assigned to "1" when the pulse amplitude is above the threshold voltage. In other case, when the pulse amplitude is lower than threshold voltage, the pulse is assigned to "0". During recovery of the received data, CDR decides at the midpoint of each pulse in order to lower bit-error-rate (BER).

In addition to low power and single supply operation, TIA must exhibit linear phase response in order to be used for 10 Gbit/s applications. Trade-off between noise, speed, gain and supply voltage presents many challenges in TIA design. Overall sensitivity of the receiver is mostly determined by TIA because TIA is the first electrical part after photodiode. That being the case, TIA must maintain a reasonable signal gain as well as producing little noise to improve the sensitivity. It is also desirable to accommodate wideband data extending from almost dc to high frequencies to avoid intersymbol interference (ISI), which lowers BER. As performance indicators, BER is used to determine the bandwidth and the sensitivity, and the eye diagrams can be visual aids to estimate or to troubleshoot sources of noise and the other limiting factors. To meet these requirements, this study presents a new topology and compares it with the other transimpedance amplifier topologies.

In this thesis, the differential SiGe transimpedance amplifier for 10 Gbit/s fiber optical receivers is realized and its results are presented. The TIA is optimized for the best phase linearity over the bandwidth resulted in a group delay variation less than 1 ps. No inductor is used to achieve wideband operation. SiGe HBT BiCMOS enables TIA to be a cost-effective alternative and to integrate with other blocks of the fiber optical receiver. The differential structure of the TIA makes it immune to the effect of the supply and substrate noise. While flat frequency response with 9 GHz bandwidth is obtained, differential transimpedance gain is almost 58 dB $\Omega$ . The electrical sensitivity of the proposed TIA is 15  $\mu\text{A}_{\text{pp}}$ . Power consumption is 71 mW and maximum differential output swing is 320 mV $_{\text{pp}}$ . It is shown that the differential TIA is well suited for 10 Gbit/s data rate and OC-192 specifications.

## 10 Gbit/s FİBER OPTİK ALICILAR İÇİN SiGe BiCMOS FARKSAL GEÇİŞ-EMPEDANSI KUVVETLENDİRİCİSİ TASARIMI

### ÖZET

1970'lerin başında silika fiberin kaybının 20 dB/km düzeyinin altına indirilmesi sonucunda, telekomünikasyon sektöründe ve daha sonra internet ve veri paylaşımı alanında fiber optiğin payı yıllar ilerledikçe artmıştır. Şüphesiz bunda etkili olan en büyük nedenler; ışığın kullanılmasıyla gerçekleştirilen veri transferinin EMI'den çok az etkilenmesi, çapraz-geçişin (cross-talk) çok az oluşu, düşük üretim ve montaj maliyetleri ve de dayanıklılık gibi fiber kablunun sağladığı üstünlüklerdir. Fiber optiğin en azından teorik olarak hali hazırda çok büyük bant genişliği sağlayabilmesi ve büyük veri taşıma sığası sunması, daha hızlı uç elemanlarına ve elektronik tümdevrelere gereksinim olduğu gerçeğini de beraberinde getirmiştir.

Yarıiletken teknolojisindeki yeni gelişmeler sonucu ortaya çıkmış bulunan heterostructure" ve "heterojunction" yarı iletken devre/kırmık elemanları, fiber iletişimin öngördüğü hızlı veri taşıma ve düşük gürültü özelliğini bir arada sunabildiklerinden, fiber optik alıcı ve vericilerinin uç elemanları olarak geniş kullanım alanı buldular.

SiGe çift kutuplu (bipolar) tranzistorunun geliştirilmesiyle, bu teknoloji ürünü tranzistorlar, fiber optik alıcılarında uç elemanı olarak kullanımlarında önem kazanmışlardır. SiGe teknolojisi, çift kutuplu Si tranzistorun Baz bölgesine belirli oranda Germanyum katkılanmasıyla, aynı boyutlardaki bilinen çift kutuplu tranzistora (BJT) göre daha büyük  $f_T$  kesim sıklığı olanağını sunmuştur. Baz bölgesi dağılmış direncinin de daha düşük değerlere düşmesi sonucunda da, daha düşük gürültülü uç elemanlar gerçekleştirilmesine olanak sağlamıştır. Bu üstünlükleriyle SiGe, yukarıda sözü edilen III-V ve HBT yapılarıyla rekabet etme şansı bulmuştur. Ardından SiGe BiCMOS teknolojisi, alıcının analog ve sayısal tüm öbeklerinin aynı kırmık üzerinde tümleştirme olanağını da sunabildiğinden, düşük gürültülü, geniş bantlı ve düşük maliyetli çözümler gerçekleştirilmede söz konusu alanlar için çok çekici olmuşlardır.

Vericideki lazer diyot aracılığı ile sayısal veri, ışık kaynağına dönüştürülür ve fiber kabloya gelir. Fiber kablo içinde yitime ve dağılıma (dispersion) uğratılan, modüle edilmiş (kodlanmış), sayısal bilgi taşıyıcısı ışık, alıcıdaki foto diyot tarafından yeniden elektrik akımına dönüştürülür. Burada bu elektrik akımı, önce TIA tarafından yükseltilip kendisiyle orantılı gerilime dönüştürüldükten sonra, ikincil kuvvetlendirici ile (post amplifier, PA) genliği daha da artırılarak saat devresine (clock and data recovery, CDR) gönderilir. Saat devresinde saat işareti ve veri bilgisi ayrıştırılır ve daha küçük hızlara azaltılmak için "DEMUX" devresine gönderilir. CDR bir eşik gerilimi üretir. Bu eşik geriliminin üzerindeki genlik sayısal "1", altındaki genlik sayısal "0" olarak belirlenir. Burada CDR, bu süreci gerçekleştirmek için her bir darbe süresinin tam ortasında karar verir. Bunu yapmasının nedeni dağılıma ve bozunuma uğratılmış işarettaki farklılaşmaları göz önüne alarak en güvenli bit çözümlemesini gerçekleştirmesidir.

Bu noktada TIA tasarımının büyük önemi bulunmaktadır. Çünkü TIA işaretin foto diyottan sonra uğradığı en ön kattır ve bütün alıcının gürültüsünü büyük oranda bu katın gürültüsü belirleyecektir. Dolayısıyla gerçekleştirilecek TIA'nın düşük gürültülü

olması gereklidir. Dağılım/bozunum etkilerinden kaynaklanan kare dalgadaki bozulmalar, gürültünün de etkisiyle her bir darbenin CDR tarafından yanlış çözümlenme olasılığını artıracaktır. Bunun önüne geçmek için alıcının duyarlılığı belirli bir hata payı üzerinden hesaplanır. Doğal olarak, TIA'nın bu duyarlılığa etkisi büyüktür. Bu duyarlılık, fiber iletişim kurallarının belirlediği bit-hata-oranı (bit-error-rate, BER) üzerinden hesaplanır ve göz diyagramları (eye diagrams) çıkıştaki işaretin ne derece düzgün olduğunu görmemizi sağlar.

Bu projede 10 Gbit/s gibi hızlı bir uygulama hedeflendiğinden TIA'nın geniş bantlı olması gerekeceği açıktır. Bu düzeydeki bir hızla modüle edilmiş işaret; bant genişliği yeterli olmayan bir TIA'ya uğradığında, işaretle bozulmalar meydana gelecek ve göz diyagramında yatay ve dikey kapanmalar gözlenecektir. Bununla birlikte gereğinden fazla bant genişliği girişte daha büyük toplam gürültüye neden olacağından, TIA'nın bant genişliği ve gürültüsü arasında bir uzlaşının sağlanması gerektiği açıktır. 10 Gbit/s NRZ koduna sahip veri işareti için yaklaşık 7 GHz bant genişliğine sahip bir uç devresi fiber optik alıcılar için yeterli olabilmektedir.

Sıklık (frekans) domenindeki düzgün sıklık tepesi ve yeterli bant genişliği ölçümleri, çıkıştaki işaretin şeklinin düzgün olabilmesi için yeterli değildir. Dolayısıyla işaretin evresindeki (phase) değişimler de gözlemlenmelidir. Yeteri kadar doğrusal olmayan evre tepesi ya da düşük evre paylı işaret, geçici rejim (transient) ölçümlerinde aşımara neden olabilmektedir.

Gürültü ve hız arasındaki optimizasyonda TIA'nın kazancı, düşük güçlü ve tek besleme kaynağına sahip olması gibi diğer önemli ve ayırt edici özelliklerin de eklenmesiyle, TIA tasarımında bu özelliklerin arasından istenen hız için en optimum performansı sağlayacak sonuçlar elde edilmeye çalışılmalıdır. Çünkü sahip olunan yarı iletken teknolojisinin özellikleri ulaşılabilecek performansı büyük ölçüde belirlemektedir.

Büyük geçiş-empedansı (transimpedance) kazancı elde etmek aynı zamanda büyük bant genişliği elde etmeyi sınırladığından genellikle ikincil kuvvetlendiriciye ihtiyaç duyulur. Bu ikincil kuvvetlendiriciler farksal yapıya sahiptir. CDR'deki veri çözümlenme işlemi için birkaç yüz mili volt yeterli olabilmektedir. Dolayısıyla TIA'dan elde edilecek 50-60 dB $\Omega$  mertebelerindeki kazanç ilaveten 30-40 dB aralıklarında ikincil kuvvetlendiriciye ihtiyaç olacaktır.

TIA'nın fark kuvvetlendiricisi şeklinde tasarlanması güç kaynağı dalgalanmalarını, ortak biçim gürültüsünü ve parazitik etkenlerin neden olabileceği kararsızlık sorunlarını büyük ölçüde giderir. Aynı zamanda ikincil kuvvetlendiricide ayrıca bir referans gerilim üreticini gerekli kılmaz. Bu anlamda farksal yapıyı ihtiva eden TIA tekil yapıya göre daha avantajlıdır. Ancak farksal yapıdaki ilave tranzistorlar ve tümdevre elemanları, gürültünün artmasına dolayısıyla duyarlılığın kötüleşmesine de neden olacaktır. İlaveten, foto diyotun tek çıkış üretmesine karşılık TIA'nın iki girişi olması, asimetric sorunlara neden olacaktır. Bunun için bu çalışmada foto diyot TIA'nın diğer ucunda da modellenmiştir.

TIA tasarımında yukarıda belirtilen performans ölçütlerine ulaşmak için geliştirilen/sunulan değişik devre yapıları ve performans artırıcı teknikler kaynaklarda vardır. Bu çalışmada bunlara değinilmiş ancak tasarlanan devrenin iyi sonuçlar vermesiyle bu yapıları kullanmaya gereksinim kalmamıştır.

Bu çalışmada 10 Gbit/s hızındaki fiber optik uygulamaları için fiber optik alıcının en önemli katlarından birisi olan geçiş-empedansı kuvvetlendiricisi (transimpedance amplifier) tasarlanmış, devrenin benzetimleri gerçekleştirilmiş ve sonuçları sunulmuştur. Söz konusu yarı iletken teknolojisi ile en iyi devre yapıları ve mimarileri incelenmiş, analizleri ve benzetimleri yapılmıştır. En iyi sonuçlar paralel-direnç geri besleme devresi kullanılarak elde edilmiştir.

DüĖgün bir sıklık tepesi ile 9 GHz kesim frekansı elde edilmiştir. İlaveten, oldukça doğrusal evre tepesi sonucuna ulaşarak, 1ps den daha az grup gecikmesi (group delay) değışimi elde edilmiştir. 58 dBΩ farksal TIA kazancı sağlanmış ve 1.061 μA toplam giriş gürültüsü ile 15 μA<sub>pp</sub> elektrik duyarlılığı elde edilmiştir. En yüksek farksal çıkış işareti salınımı 320 mV<sub>pp</sub>'dir. Güç tüketimi tek besleme kaynağından, 3.3 V ile 71 mW'dır. Her bir TIA tasarımı için ayırt edici ölçüt olan ortalama giriş gürültüsü 11.18 pA/√Hz'dir. Gerçeklenen TIA, PA ile aynı kırmık içinde gerçeklenmemesi durumunda, S<sub>22</sub> benzetimi 1 GHz ile 9 GHz arasında -15 dB'in altında kalacak şekilde elde edilmiştir. Gerçeklenen devre 10-Gbit/s hızı için ve SONET OC-192 standartları için uygun bir devredir.



## 1. INTRODUCTION

The growth of telecommunication and the surge in data communication mandates the use of broadband communication systems. Fiber optical communication systems have been an attractive solution to cope with the high-speed data rates and to transport the huge amount of data capacity for both long-haul and short-haul transmission systems. Together with the high-speed HBT and III-V technologies (later deep submicron CMOS has taken place in this race), light transmission through fiber has made an incredible progress in the telecommunication field and internet.

Until recent years, high cost, high power III-V devices (GaAs MESFETs, AlGaAs/GaAs HEMTs, AlGaAs/GaAs HBTs) have occupied fiber optical receivers since they present very high bandwidth solutions. Recently, SiGe technology has taken the place, which exhibits large  $f_T$  as well as performing low power and low noise behavior. With the employing of SiGe BiCMOS technology; low-cost, high-performance integrated fiber optical receivers come into prominence.

An optical receiver converts the optical signal received at the output end of the optical fiber back into the original electrical signal. The illustration of optical receiver is given in Figure 1.1. As being the first building block after photodiode, transimpedance amplifier (TIA) amplifies electrical current with sufficient bandwidth, converting it to a voltage, while adding as little noise as possible. That being the case, TIA is without a doubt the most critical building block of the optical receiver. The design of this block involves many trade-offs between noise, bandwidth, gain and stability. This dissertation tries to reveal all subtleties and challenges encountered during the design of low-noise, high-bandwidth differential TIA.

The most common TIA configuration is the shunt-feedback TIA topology, where a negative feedback network senses the voltage at the output and returns a proportional current to the input. This type of feedback is chosen in this study because it shows very good performance for the given technology and it is well suited for intended speed.

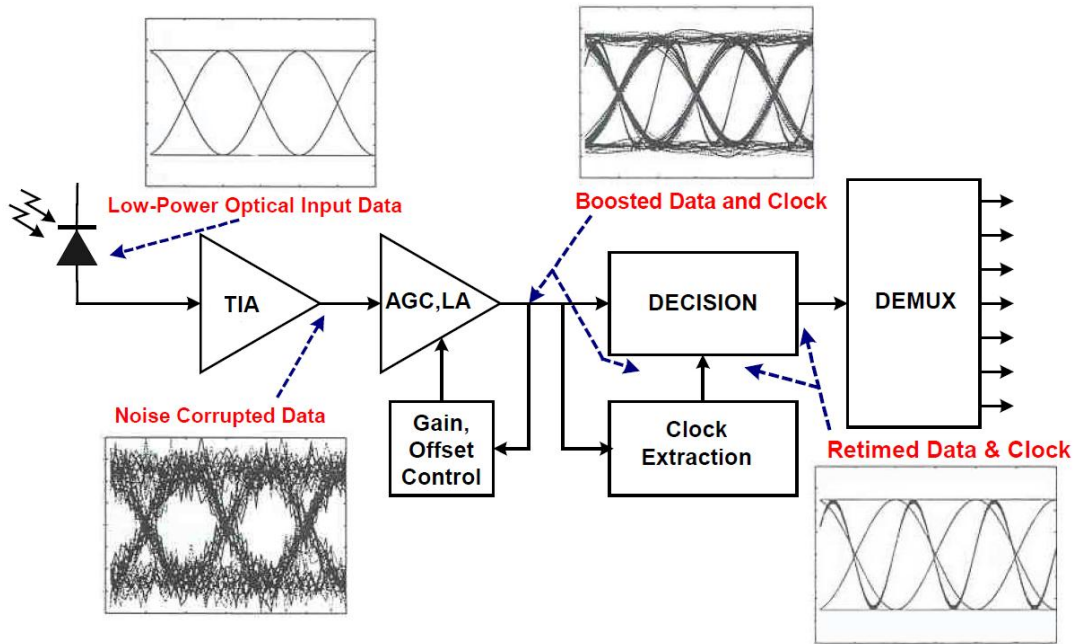


**Figure 1.1:** Illustration of fiber optic receiver.

## 1.1 Purpose of the Thesis

The purpose of this thesis is to accomplish a transimpedance amplifier for the 10 Gbit/s fiber optical receivers. The goal is to provide output signal having wide bandwidth and low-noise as well as sustaining suitable gain. Even if required cut-off frequency for the 10 Gbit/s NRZ data rate is about 7 GHz, 8-9 GHz bandwidth is intended. Since required signal amplitude for the data recovery is several hundreds millivolts, transimpedance gain between 50-60 dB/ $\Omega$  gain is aimed. The remaining gain has to be carried out at the post amplifier because of tight noise and bandwidth restrictions stemming from TIA design. Differential topology is another scope to eliminate common-mode noise. Semiconductor technologies including CMOS will make presented TIA easily to combine with subsequent stages of the receiver and thus SiGe BiCMOS process is preferred for this work.

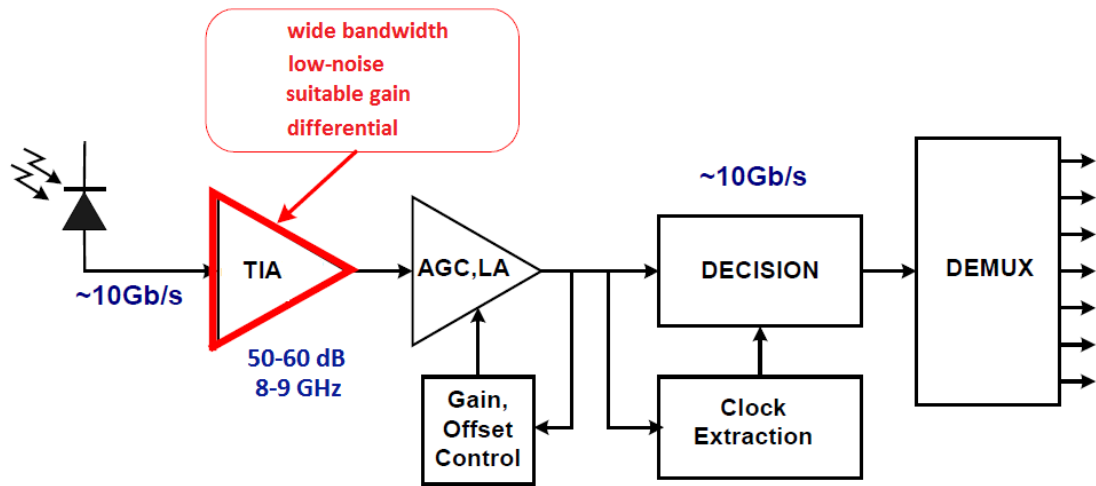


**Figure 1.2:** Transimpedance amplifier design.

## 1.2 Thesis Outline

This work presents a differential, broadband and low-noise transimpedance amplifier for 10 Gbit/s fiber links using SiGe HBT BiCMOS process.

In Section 2, some important information about the fiber communication is given. Fiber optic receiver components such as fiber optic cable and photodiode specifications are also investigated.

Section 3 provides background and theoretical basics as well as resolving the evolving design complexity. Receiver fundamentals such as BER are explained. The most important TIA specifications are emphasized. Finally, TIA circuit types are searched for the best circuit performance.

In section 4, design platform and technology process are discussed. Explanations about the methodology to achieve projected performance are provided. The proposed TIA is investigated and the design is achieved. After the realization of the theoretical circuit, results are presented. Eventually, conclusions and further explanations are covered in Section 5.



## **2. FIBER OPTICAL COMMUNICATION SYSTEM**

The rapid rise of internet traffic and the need for high capacity data transmission for local area networks have made optical communications the best choice for high speed data transmission. Compared to the conventional electrical communications, the communication using optical carrier waves is usually immune to electromagnetic interference and cross talks, offers very high bandwidth usage, provides low transmission losses at very high frequencies, includes good overall system reliability and maintenance. Free space RF transmission is flexible and cheap, but it cannot support large bandwidths and requires fairly large power to transmit over long distances. Free space optical transmission is also quite flexible, but the signal quality and propagation distance are weather-dependent. Standard RF signal propagation over coaxial cable is simple to integrate with standard electronics and is ideal for relatively short distances and low data rates [1]. Due to the advantages stated above, fiber optical transmission system is widely realized in areas such as long-haul transmissions, local area networks, inter-city telecommunication, cable TV etc.

The Synchronous Optical Network (SONET) and Synchronous Digital Hierarchy (SDH) standard govern the fiber optic transmission schemes. While SONET regulates the requirements in the USA, SDH standards are for Japan and Europe zone. These standards define the technology, performance and specifications required by the fiber optical systems through a synchronous, flexible, optical hierarchy by means of multiplexing scheme [2], which is shown in Table 2.1.

These transmission data rates and their standards have been issued over the years as the need for high capacity traffic is increased. Since the intended speed of this design is 10 Gbit/s, OC-192 hierarchy specifications are to be cared.

**Table 2.1:** SONET/SDH hierarchy.

SONET	SDH	Bit Rate
OC-1	-	51.84 Mbit/s
OC-3	STM-3	155.52 Mbit/s
OC-12	STM-4	622.08 Mbit/s
OC-48	STM-16	2.4883 Gbit/s
OC-192	STM-64	9.9533 Gbit/s
OC-768	STM-196	39.8131 Gbit/s

A figure to give a quick understanding about conversion of data between electrical signal and light is shown in Figure 2.1. The modulation of the data to light takes place at the optic transmitter. The laser driver converts the data, in the form of an electrical signal, to current. Light is produced with the current responding the laser diode. The data-modulated light is channeled to the receiver via a fiber guide. The receiver uses a photodiode to convert the incoming light to current. The data is recovered by two amplification stages: Transimpedance amplifier (TIA) and post amplifier (PA). TIA, which is the main target of this thesis and will be largely discussed in the next, converts the current to a low-noise voltage signal.

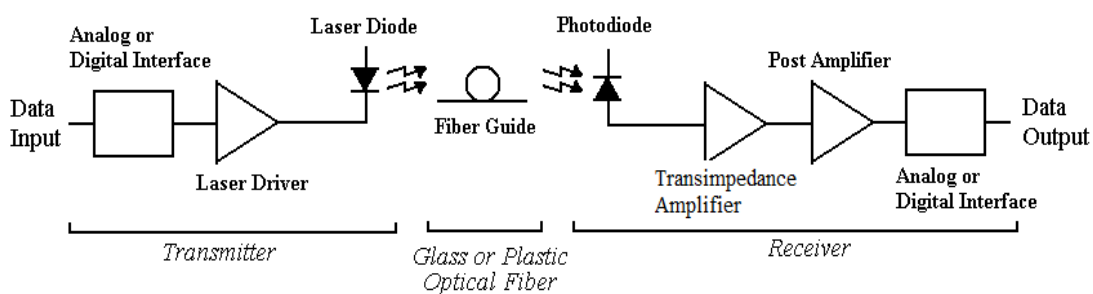


**Figure 2.1:** Fiber Optical Communication system.

Depending on whether the optical signal is transmitted over relatively long or short distances, fiber communication transmission can be classified into two categories: long-haul and short-haul communications. Long-haul communication systems (like inter-continents) require high capacity, high bandwidth trunk lines. Periodic regeneration and amplification of the optical signal by using repeaters (both

electronic and optical amplifiers) is still required for most long-haul systems. Short-haul communication applications cover intercity and local-loop traffic. Such systems operate at lower bit rates over distances of less than 50 km [2].

The data transport capacity of a single fiber is improved by applying Wavelength Division Multiplexing scheme (WDM), which simultaneously transmits many data streams on to the single fiber at different wavelengths. Although the WDM scheme described above provides large data shipping ability, there are some technology limitations in providing a number of wavelengths, such as channel broadening effects, non-ideal optical filtering and the limited channel wavelength spacing for the desired performance.

There are mainly two types of modulation format used in optical fiber communication: *Non-return-to-zero (NRZ)* and *return-to-zero (RZ)*. The NRZ is a kind of on-off keying, meaning the signal is *on* to transmit the “one” bit and is *off* to transmit the “zero”. In RZ, however, the data returns to “zero” after every bit to allow safe propagation of pulses. As it is seen from the Figure 2.2, the duration of “one” pulses (half of the pulse duration of NRZ) are less than that of NRZ. Therefore, RZ format tolerate pulse spreading and intersymbol interference (ISI) due to the dispersion, allowing better decision threshold. It is used in long-haul systems due to the dispersion performance.

As it will be dealt with in the following chapter, NRZ signal enables front-end of the receiver to have lower bandwidth (BW) for the same data rate ( $B_R$ ). The bandwidth is  $0.7B_R$  in NRZ while it is approximately two times the bit rate in RZ modulation. This specification makes the NRZ the most commonly used one at 10 Gbit/s applications [3, 5]. During the whole design, NRZ modulation format is taken into account.

Right before digital data is modulated on optical carrier, they are usually preconditioned dictated by SONET specifications. The preconditioning, namely line coding, provides transmitted bit stream to have the properties such as short run lengths and high transition density. It is desirable to control the number of successive zeros and ones for the small value. This approach limits the *DC wander* effect allowing the use of AC coupling in receiver design. In SONET specifications, generally, more than 72 consecutive bits are not allowed and this condition is sustained using scrambling.

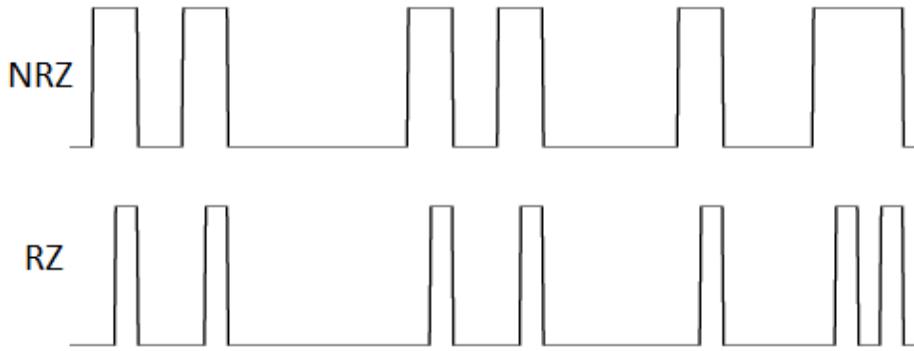


**Figure 2.2 :** NRZ and RZ data modulation.

## 2.1 Fiber Optic

Figure 2.3 depicts the cross-section of fiber structure. In its simplest form, an optical fiber consists of a cylindrical core of silica glass surrounded by a cladding whose refractive index is lower than that of the core. The outer jacket is called the cable, which acts as waveguides for the optical signal. The cable can contain one or more fibers.

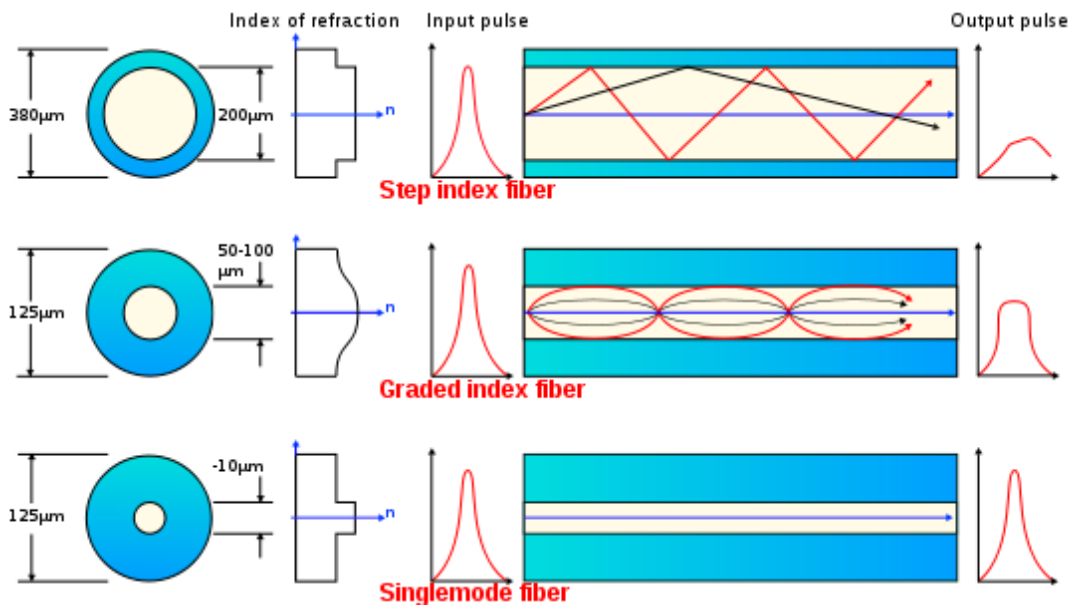


**Figure 2.3:** Cross-section of fiber and fiber types [6].

The role of a communication channel is to transport the optical signal from the transmitter to the receiver with as little loss and dispersion as possible. Like other communication channels, fiber cable also attenuates the signal, which is called the fiber loss due to the scattering, absorption by material impurities or other effects. In 60s, when the fiber was first presented, the loss was about 1000 dB/km. it was

during 70s that low loss fiber (less than 20 dB/km) started to be produced, which made the fiber an important candidate for the broadband communications. Today, silica fiber loss is around 0.18-0.2 dB/km [7].

The short history stated above is for the silica-based fiber. There is another type of fiber having much amount of loss (55 dB/km) is the plastic fiber. The plastic optical fiber bears the advantage of low cost, enduring and ease implementation such that they are mostly preferred for very short applications.

Dispersion, which is actually a kind of distortion, is the broadening of individual optical pulses during propagation through the fiber. If optical pulses spread significantly outside their allocated bit slot, then the transmitted signal is severely degraded. Eventually, it becomes impossible to recover the original signal with high accuracy at the decision circuit. This unwanted phenomenon appears as ISI and jitter on the eye diagrams.

The silica glass has two low loss operating wavelength windows. One is around wavelength  $\lambda=1.3 \mu\text{m}$  and the other one is at  $\lambda=1.55 \mu\text{m}$ . At the  $1.55 \mu\text{m}$  wavelength, silica fiber has the lowest loss which is about 0.2 dB/km whereas it is about 0.4 dB/km for the  $\lambda=1.3 \mu\text{m}$  medium. However, the dispersion is lowest at the  $1.3 \mu\text{m}$  window [5]. The operating region of plastic fiber is  $0.75\text{-}0.82 \mu\text{m}$  while maintaining lowest dispersion in this window as well.

Fiber optic cable can also be classified according to the operating mode. When the only one ray light propagates through the fiber at only one path, it is called single mode fiber. As it is seen from the Figure 2.3, multimode fibers have relatively bigger core allowing the light to take multiple pathways. That multimode operation increases the data capacity of the channel. Dispersion issue is the most severe in the case of multimode fibers since pulses spread rapidly because of different speeds associated with different fiber modes. It is, for this reason, used for shorter distances. Most optical communication systems use single-mode fibers because single-mode fibers are better at retaining the originality (or shape) of each light pulse over long distances than multimode fibers [2].

## 2.2 Photodiode

The first part of an optical receiver is the photodetector. The photodiode is a square law device, which means that the detected electrical current depends on the power of the incident optical signal. The main characteristics of this device are its responsivity, speed and the leakage current. As it is given and plotted in section 3, the receiver's sensitivity is largely determined by the capacitance of the photodetector together with the input impedance of the transimpedance amplifier.

Semiconductor photodiodes are used in fiber optical receivers as photodetectors because of their compatibility with the whole system. Phototransistor is not preferred in high-speed applications due to the high base-collector junction capacitance  $C_{\mu}$ . PIN (p-i-n) photodiode is widely used in high-speed applications (2.5-40 Gbit/s). Figure 2.4 illustrates structure and approximate small-signal model of a PIN photodiode.

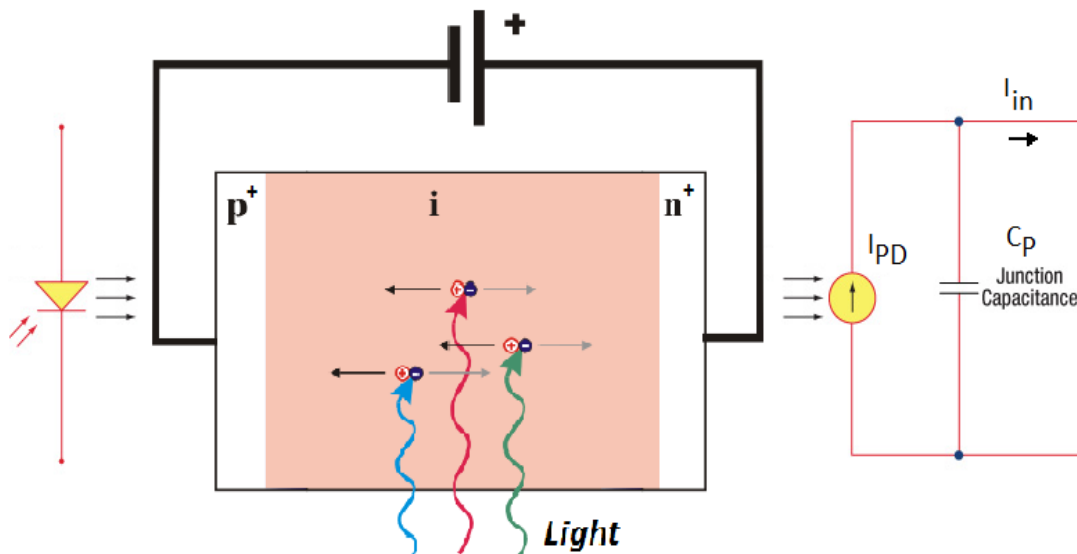


**Figure 2.4:** PIN Photodiode and approximate small-signal model.

In the intrinsic region or depletion region (undoped or lightly doped), the conversion of the light to the electric current occurs by means of absorbing photons. Photons incident on i-layer creates electron-hole pairs. Reverse biased p-doped  $p^+$  and n-doped  $n^+$  regions creates strong electric field in the depletion material. Because of this strong reverse polarization, separated electron and holes created by light are absorbed to opposition polarities producing continuous current. Ideally, every photon must create an electron-hole pairs. However, due to the reasons such as thermal

effects, absorption imperfections, this condition cannot be met. This is called quantum efficiency,  $\eta$  [2].

Semiconductor photodiodes used in photoreceivers have operating wavelength at which they absorb photos in accordance with their quantum efficiency. Table 2.2 gives operating wavelength of the most available photodiodes types. Because of the operation principals of light in a medium, photodiode choice is not an easy choice for the designer. For instance, for the high-speed silica glass fiber, InGaAs photodiode is a popular choice because of its high performance [8].

**Table 2.2:** PIN Photodiode operating wavelengths.

Semiconductor	Wavelength
Silicon	750-850 nm
Germanium	1100-1600 nm
GaAs	700-850 nm
InGaAs	1100-1700 nm
InGaAsP	1100-1600 nm

In the small-signal model of Figure 2.4, photodiode is modeled only with p-n junction capacitance,  $C_p$ . This model is enough for the simulation and design performance because the intrinsic resistance of contacts and bond wire is too small that it can be ignored. Likewise, shunt junction resistance can be ignored because of the wide intrinsic region [9]. As it will be stated in the following, the input impedance of the TIA is the most important design criteria, which is mostly determined by  $C_p$ . To get intuitive understandings about sensitivity given in the next section, it is helpful to give figure-of-merit equation of PIN photodiode. It is [9]

$$I_{pD} = \mathcal{R} \cdot P \quad (2.1)$$

Where  $I_{pD}$  is the photodiode current produced for a given amount of optical power  $P$ .  $\mathcal{R}$  is the responsivity of PIN photodiode given by

$$\mathcal{R} = \eta \frac{\lambda q}{hc} \quad (2.2)$$

Where  $q$  is the electric charge,  $h$  is the Planck constant;  $c$  is the speed of light in vacuum. The responsivity of typical InGaAs PIN photodetector is typically in the range of 0.6 to 0.9 A/W [10].

Noise of the shunt resistance and series contact resistance can be ignored due to high and small values, respectively (thermal noise of resistor will be dealt with in the following). Besides, there is also shot noise and thus the noise on “ones” is larger than the noise on “zeros”. Another demerit is dark current or leakage current. Even if photodiode is not illuminated, very small value of current can leak from the photodetector.

### 3. BACKGROUND, THEORY AND DESIGN CONSIDERATIONS

The huge data transport capacity of the fiber communication system practically cannot be fulfilled because this theoretical broadband operation is limited by the speed of front-end circuits. That is why their design is the most vital one of the optical transceiver design. III-IV devices and heterojunction bipolar transistors (HBT) with very high transition frequency are widely incorporated in this area to accommodate high bandwidth operations [11-13]. Although it has low gain capability compared to its counterparts, scaling-down of the CMOS technology makes CMOS a low cost, low power choice [14]. Combining SiGe HBT with CMOS (BiCMOS technology) allows this technology to take advantage in this race. SiGe HBT has recently provided a cost-effective alternative and higher integration levels, especially in BiCMOS process, with improved sensitivity for 10 Gbit/s fiber optical front-ends and for the development of photoreceivers [15-16].

Before beginning to investigate design issues, it will be instructive to look at overall receiver system. Block diagram of a typical fiber optical receiver is shown in Figure 3.1. The optical signal is detected and converted to an electrical current by a photodetector. As mentioned in the previous section, semiconductor photodiodes are used as photodetectors because of their compatibility with the whole system. A TIA converts the electrical current to a voltage and amplifies it. This quantity of amplification is not sufficient for signal processing. Therefore, right after TIA, a post amplifier (PA), which is also a voltage amplifier, amplifies the signal to the higher amplitudes. This allows the data pulses coming from fiber transmission safely to be detectable and processed at the subsequent stages. PA could be in the form of automatic gain control amplifier (AGC) enabling transimpedance gain of the front-end to be lowered for large input signals or in the form of limiting amplifier (LA) which limits the output signal for large input signals. If low distortion is strictly necessary, then AGC must be preferred. In other case, where distortion can be ignored, then LA is preferred because of its simplicity.

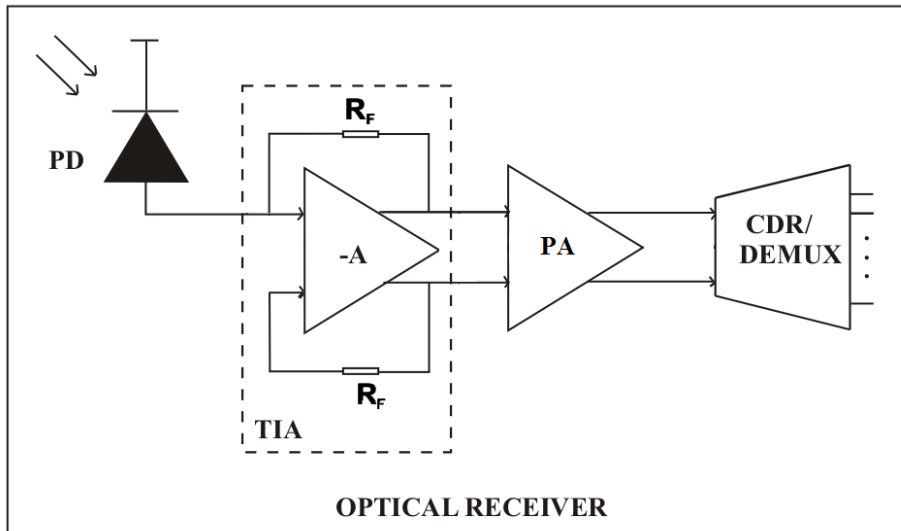


**Figure 3.1:** A typical fiber optical front-end with shunt-feedback TIA.

Clock and data recovery (CDR) extracts the digital data and clock information from the received signal. This is done by defining threshold voltage. The pulse is assigned to “1” when the pulse amplitude is above the threshold voltage. In other case, when the pulse amplitude is lower than threshold voltage; the pulse is assigned to “0”. During recovery of the data from the received signal, CDR decides at the midpoint of each pulse in order to lower bit-error-rate (BER). The recovered data is finally demultiplexed as parallel channels having lower data rates.

This section will give an explanation about the requirements and challenges faced during the design of 10 Gbit/s SiGe differential TIA. Merits and demerits of the circuit topologies are investigated for the required performance. At first, TIA performance specifications are analyzed. Later, typical TIA circuit topologies are discussed to give an understanding about presented TIA circuit. Finally, SiGe HBT transistor description is briefly pointed out.

### 3.1. Design Requirements

Like all other analog amplifiers, optical amplifier has limited dynamic range. This dynamic range has lower and upper corners determined by the several effects. The lower end of an optical receiver is restricted by sensitivity. As it will be seen in the following paragraph, sensitivity is determined by the total integrated input-referred noise at the input of the receiver. Since TIA is the first amplifier block, the overall noise of the receiver is mostly determined by TIA. The upper corner is restricted by input overload current after which signal patterns exhibits considerable distortion. These properties make TIA design an important one.

### 3.1.1. Sensitivity and bit-error-rate

A receiver is said to be more sensitive if it achieves the same performance with less optical power incident on photodiode. The launched optical power is therefore an important parameter because it indicates how much light arrives at the surface of the photo detector. The signal uses digital discrete modulation of optical field. The receiver recovers a sequence of binary digits from the incoming optical signal, thus, the technique used to specify a digital receiver's sensitivity is different from that used for an analog receiver. The primary measure of the performance of such systems is to quantify the probability that the receiver will make an incorrect decision. Therefore, bit-error-rate (BER) is defined as the ratio of number of incorrect identifications to total number of bits recovered at the decision circuit of the receiver. For example, a BER of  $10^{-9}$  corresponds to on average of one error per billion bits. The SONET OC-192 standards specify a BER of  $10^{-12}$  as the minimum operating requirement [16].

Without quantifying BER, sensitivity itself cannot say anything. To calculate sensitivity and BER, a noisy transimpedance (noise is referred to the input) amplifier with input and output waveforms are shown in Figure 3.2. The noise signal  $\bar{i}_n$ , NRZ data signal  $i_{in}$  is applied to the input of TIA. The output is amplified by TIA and converted to the voltage  $v_o$ .  $\overline{v_{n,tot}}$  represents total noise (or rms noise) both on "ones" and on "zeros". The error probability of the received bit stream at the decision circuit is represented in Figure 3.3.

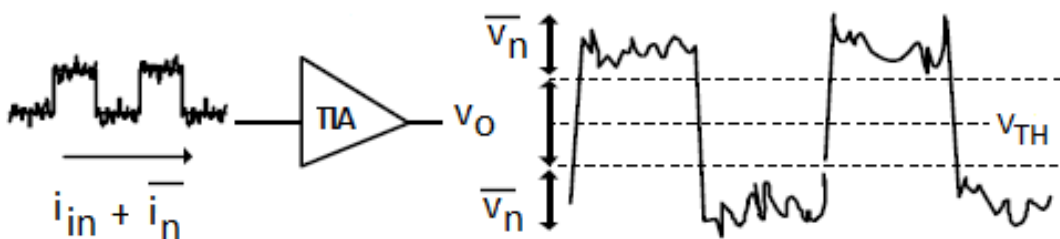


**Figure 3.2:** Relationship between signal, noise and bit-error-rate.

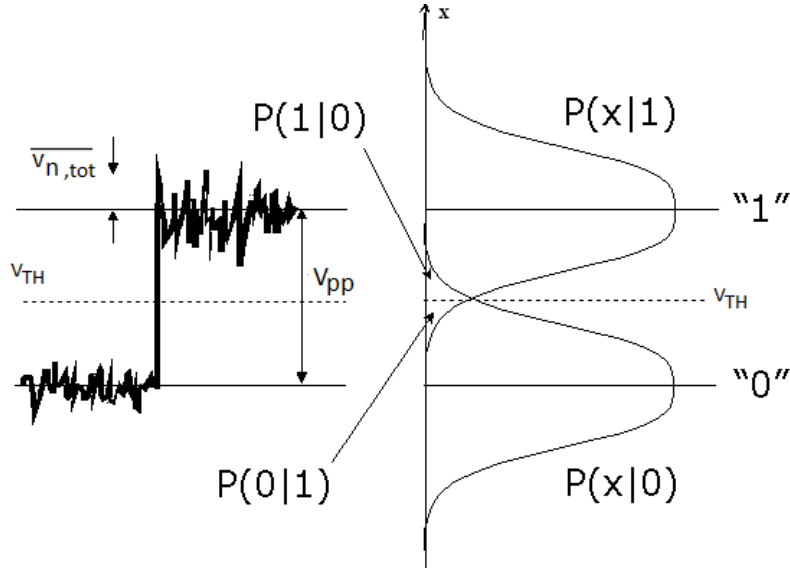


**Figure 3.3:** Bit error probability at the CDR.

The bit recovery and separation is performed at CDR by defining  $V_{TH}$ . If the addition of noise to the output voltage corrupts this certainty, and if the noise fluctuation is large enough, a binary “one” can be misinterpreted as a binary “zero” and vice versa. In order to determine if a binary bit is a “one”, or a “zero”, the signal is sampled midway through the period of each pulse. The error probability,  $P$ , of the two-level digital signal can be expressed in terms of probabilities of:  $P(1)$  for “one” and  $P(0)$  for “zero”. Also, the conditional error probabilities,  $P(1|0)$  and  $P(0|1)$  must be taken into account. Therefore,  $P$  can be written as

$$P = P(1|0).P(0) + P(0|1).P(1) \quad (3.1)$$

To simplify calculations these assumptions are made: NRZ signal is free of distortions, and noise is Gaussian and signal independent. Besides, noise on the “ones” equals to noise on the “zeros” (in practice, noise on the ones are larger than that of zeros). Thus, by symmetry, (3.1) becomes

$$P = \frac{1}{2} [P(1|0) + P(0|1)] \quad (3.2)$$

$$= P(1|0) \quad (3.3)$$

$$= \int p(x) dx \quad (3.4)$$

The definite integral will have a lower limit equal to half the peak-to-peak value,  $V_{pp}/2$ , of the output voltage and an upper limit of infinity. Because the distribution is Gaussian, the right-hand side of the equation can be expressed as

$$P(1|0) = \frac{1}{\bar{v}_{n,tot} \sqrt{2\pi}} \int_{V_{pp}/2}^{\infty} \exp\left(-\frac{x^2}{2\bar{v}_{n,tot}^2}\right) dx \quad (3.5)$$

$$= \frac{1}{2} \operatorname{erfc}\left(\frac{V_{pp}}{\bar{v}_{n,tot} 2\sqrt{2}}\right) \quad (3.6)$$

Where *erfc* stands for complementary error function, defined as

$$\operatorname{erfc}(x) = \frac{2}{\sqrt{\pi}} \int_x^{\infty} \exp(-y^2) dy \quad (3.7)$$

Hence, the error probability approximately is given by

$$BER = \frac{1}{\sqrt{2\pi}} \frac{\exp(-Q^2/2)}{Q} \quad (3.8)$$

Where

$$Q = \frac{v_{pp}}{2\bar{v}_{n,tot}} \quad (3.9)$$

Q is a measure of the ratio between signal and noise. According to the assumptions made above, that is to say; for a DC balanced NRZ signal and equal probabilities of noises, Q gives the signal to noise ratio (SNR) defined by

$$SNR = Q^2 \quad (3.10)$$

Equation (3.8) suggests that lowering the total integrated output noise voltage, or increasing the peak-to-peak signal level can reduce the BER. Although Equation (3.8) shows that we can arbitrarily reduce the BER, this is not the case in practice [17]. A BER plot for a typical receiver is shown in Figure 3.4. The BER floor indicates that beyond a certain input signal power, the BER cannot be made smaller. A further increase of signal power overloads the receiver limiting the dynamic range.

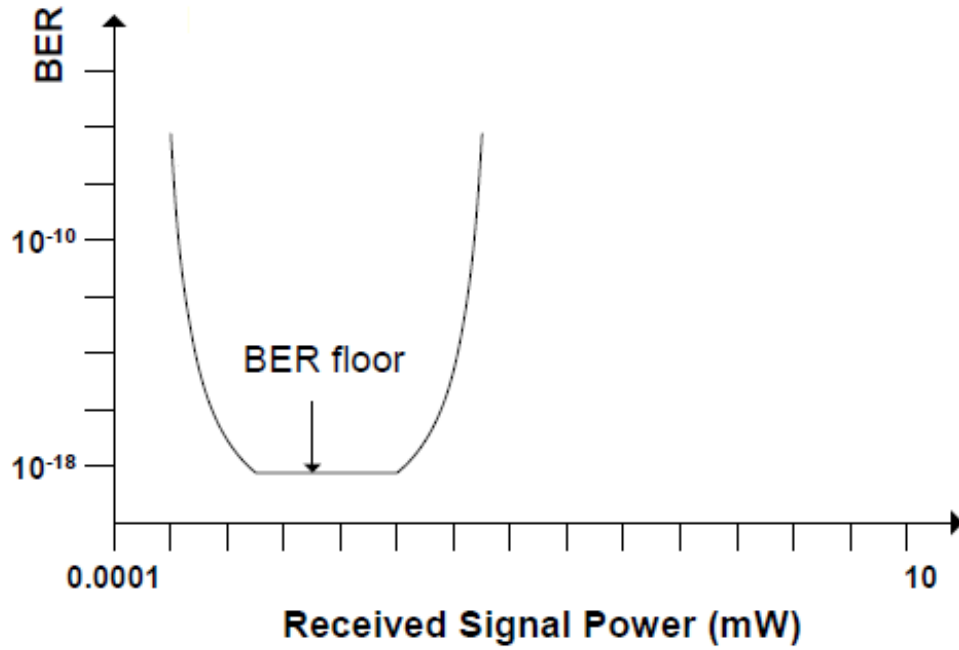


**Figure 3.4:** Practical BER curve of a receiver.

Table 3.1 shows the relationship between Q and BER. Using the Equation (3.8), at a BER of  $10^{-12}$ , the Q can be calculated as 7.035. Using (3.10), therefore, required SNR at  $10^{-12}$  BER for 10 Gbit/s speed is 16.9 dB.

**Table 3.1:** BER and Q relationship.

BER	Q	BER	Q
$10^{-6}$	4.75	$10^{-11}$	6.71
$10^{-7}$	5.20	$10^{-12}$	7.035
$10^{-8}$	5.61	$10^{-13}$	7.35
$10^{-9}$	5.99	$10^{-14}$	7.65
$10^{-10}$	6.36	$10^{-15}$	7.94

Sensitivity of an optical front-end is defined in terms of electrical and optical. Electrical sensitivity  $i_{sen}^{pp}$  is the required minimum peak-to-peak current at the input of the receiver to achieve specified BER. Likewise, optical sensitivity  $\overline{P_{sen}}$  includes responsivity of the photodiode and is defined in terms of averaged optical power

necessary to achieve minimum specified BER [10]. Peak-to-peak output voltage is equal to

$$v_{pp} = R_T i_{in,pp} \quad (3.11)$$

Where  $R_T$  is the midband transimpedance gain. Similarly, total input-referred noise current can be found using (3.12)

$$\overline{v_{n,tot}} = R_T \overline{i_{n,in,tot}} \quad (3.12)$$

Substituting Equation (3.11) and (3.12) in Equation (3.9) electrical sensitivity for a specified BER can be found as

$$i_{sen}^{pp} = 2Q \overline{i_{n,in,tot}} \quad (3.13)$$

For a DC-balanced signal averaged input current  $\overline{i_{in}} = i_{in,pp}/2$ . it is already known from Equation (2.1) that averaged optical power is

$$\overline{P} = \frac{\overline{i_{in}}}{\mathcal{R}} \quad (3.14)$$

The Equation (3.14) can be written as  $\overline{P} = i_{in,pp}/2\mathcal{R}$ . If  $i_{in,pp} = i_{sen}^{pp}$ , substituting (3.14) into (3.13) gives optical sensitivity as

$$\overline{P}_{sen} = \frac{\overline{i_{n,in,tot}} Q}{\mathcal{R}} \quad (3.15)$$

### 3.1.2. Bandwidth considerations and ISI

As briefly stated in the previous section, inter-symbol interference (ISI) can be encountered when the signal passes through the dispersive system. In fiber optical interconnection system, dispersion is associated with the fiber, transmitter and receiver circuits. ISI is that the pulses corresponding to any bit smear into the adjacent bits and overlaps. As a result, if ISI is large enough, this might trigger a false detection in the adjacent time slot. Therefore, an increasing number of errors may be encountered as the ISI becomes more pronounced. To overcome this critical issue and to evaluate the system performance, the eye diagram is a simple method to visualize the non-ideality and non-linearity in digital transmission systems [18]. Since ISI effects manifest themselves differently for different bit patterns, long sequence of random waveforms must be examined. The jitter, which is due to the variations in the pulse duration or the accuracy of the symbol clock, will cause the eye closure in the horizontal direction [18].

Since practical front-ends contain multiple poles and zeros, it is difficult to have an approach about wideband data effects or effects of the limited bandwidth of the front-end. That being the case, single-pole low-pass filter in Figure 3.5 is used to get an understanding about the relationship between bandwidth, bit rate and ISI. The input signal is periodic square wave in (a) and NRZ coded random signal in (b). Output waveforms are shown at the bottom. For a periodic square wave, low-pass filter attenuates the high frequency components causing the finite rise and fall times [19]. However, when it comes to random binary data, in which the same consecutive bits might occur, as a result of filtering effect, “DC wander” comes across. For instance, at  $t = t_2$ , together with noise, distorted output signal can be misinterpreted wrong at the recovery circuit, which may increase BER.

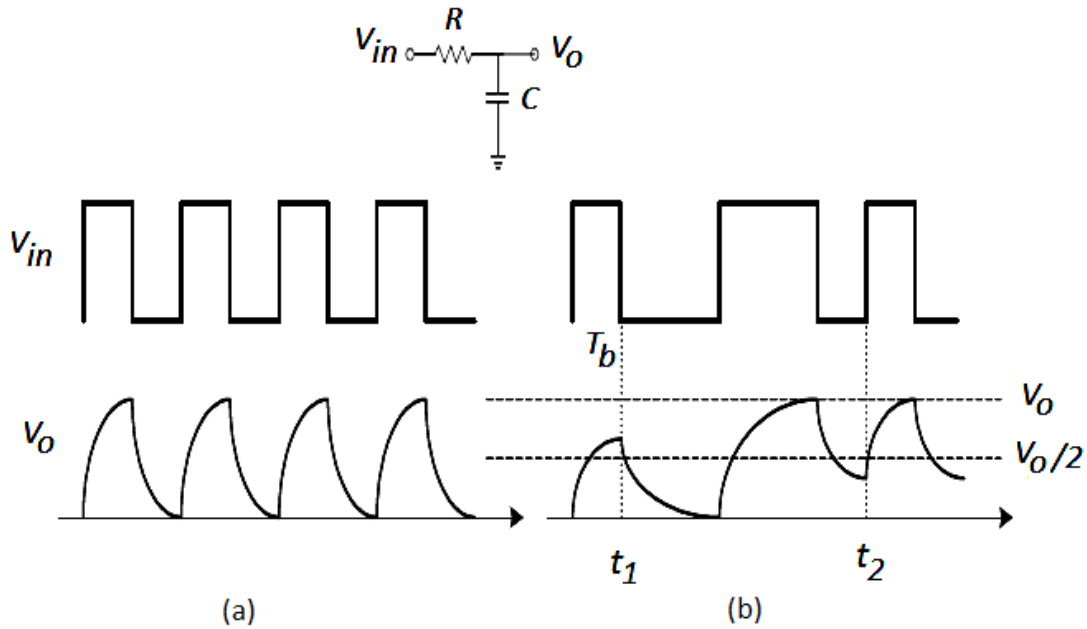


**Figure 3.5:** RC network for analyzing ISI (a) periodic square wave (b) random data.

The settling for each bit then can be expressed as [19]

$$V_o(t) = V_{in} \left( 1 - \exp\left(-\frac{t}{\tau}\right) \right) \quad (3.16)$$

Where  $\tau = RC$ . The error between  $V_{in}$  and  $V_o$  at  $t = T_b$  and the last value equals to

$$V_{in} - V_o(T_b) = V_{in} \exp\left(-\frac{T_b}{\tau}\right) \quad (3.17)$$

$$= V_{in} \exp\left(-\frac{2\pi f_{-3dB}}{B_R}\right) \quad (3.18)$$

Where  $f_{-3dB} = 1/2\pi RC$  and bit rate is  $B_R = 1/T_b$

Figure 3.6 illustrates the usefulness of the eye diagram. PRBS (pseudorandom bit sequence) NRZ data stream at 10 Gbit/s is applied to the input of the TIA having the bandwidth 4.5 GHz, 7.5 GHz and 10 GHz, respectively. The eye closure and jitter give quick information about bandwidth and noise trade-off of the receiver. As the bandwidth reduces from 7.5 GHz to 4.5 GHz, the vertical and horizontal eye closure is observed. On the other hand, as the bandwidth goes from 7.5 GHz to 10 GHz, there is no important change on the eye closure. It can be concluded from the Equation (3.18) and Figure 3.6 that higher bandwidth, after a while, does not give much effect to reduce ISI. However, bandwidth of the TIA must be minimized so as to reduce the total integrated noise and thus to improve the sensitivity. Limitation in bandwidth anyway introduces inter-symbol interference in the random data, resulting in vertical and horizontal eye closure. Hence, in order to achieve a fair compromise between the bandwidth, ISI and noise, the speed of the circuit should be sacrificed a little because in high-speed applications (2.5-40 Gbit/s), bandwidth also trades with gain and power dissipation. As a rule, the bandwidth of the front-end must be at least  $0.7B_R$  for NRZ data [20].

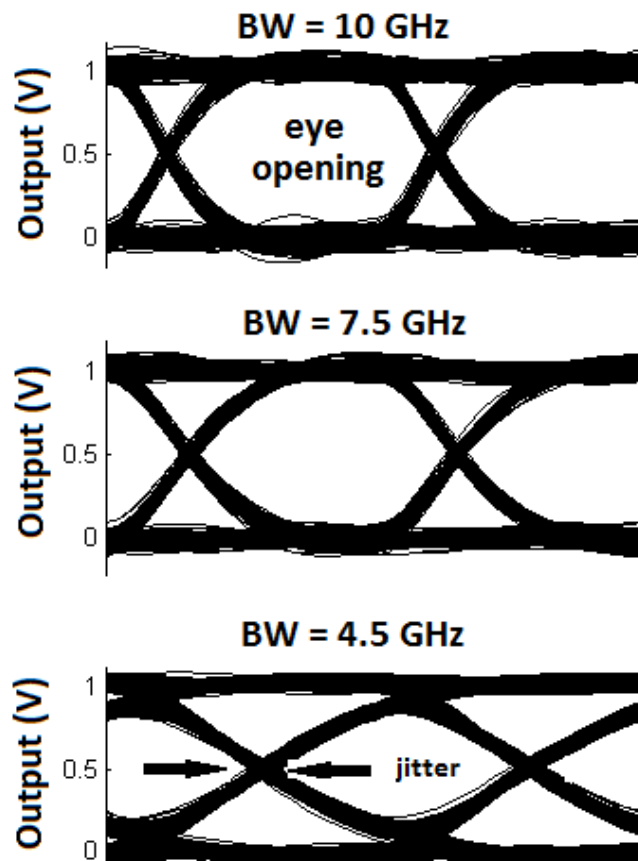


Figure 3.6: Bit rate versus bandwidth.

As the actual circuits may contain more poles (and zeros), process/temperature variations and parasitic effects mandate additional margin. Holding this reality in mind, minimum 8-8.5 GHz TIA bandwidth is targeted for 10 Gbit/s bit rate during the entire design.

To summarize what have been stated so far, for very weak signals, random noise at the receiver causes bit errors. For very strong signals, effects such as pulse-width distortion (ISI) and data-dependent-jitter cause bit errors as well. Hence, in addition to lower signal level, there is an upper signal level, known as overload limit or input overload current. Beyond this upper limit, BER requirements cannot be met as shown on Figure 3.4, which illustrates the BER plot. This definition brings the phenomenon called dynamic range. Therefore, dynamic range of a TIA is defined at its lower end by the sensitivity limit and at its upper end by the overload limit.

### 3.2 Transimpedance Amplifier Design

In Figure 3.7, typical shunt-feedback TIA is shown. Because it is located at the right after photodiode and converts electrical current to the voltage, transimpedance amplifier is the most critical and its design is the most challenging and care demanding part of the fiber optical receiver design. The design of this block involves many trade-offs between noise, bandwidth, gain and stability. The TIA is the first stage of amplification and injects the dominant noise contribution to the receiver. High gain addresses the noise issue by allowing the TIA to respond to smaller input currents. However for a given device technology, greater gain serves as an obstruction to achieving a suitable bandwidth.

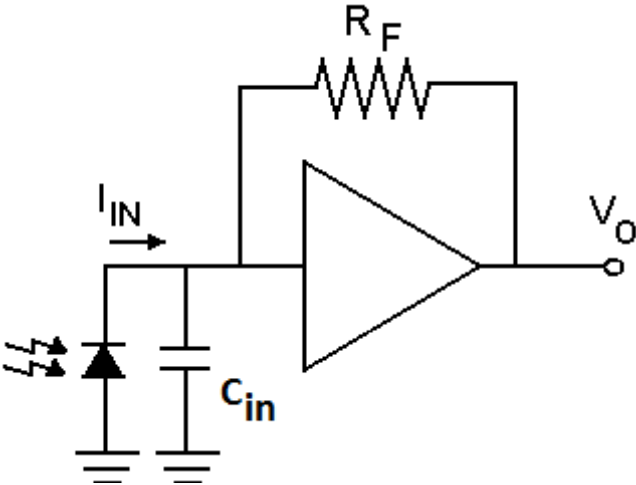


Figure 3.7: Typical shunt-feedback TIA.

Furthermore, which circuit type and technique is going to be chosen for a given technology and data rate another design challenging point. This project aims 10 Gbit/s speeds. As it will be seen in the following explanations, feedback TIA structure is the most appropriate topology to achieve wideband, low noise and enough gain.

### 3.2.1 Transimpedance amplifier specifications

#### 3.2.1.1 Transimpedance

Transimpedance gain of the TIA,  $Z_T$ , is defined as the ratio of the small-signal output voltage to the small-signal input current:

$$Z_T = \frac{v_o}{i_{in}} = |Z_T(f)|e^{j\theta(f)} \quad (3.19)$$

The higher this value, the more output signal is produced for a given input signal. The transimpedance gain is specified either in units of  $\Omega$  or  $dB\Omega$ . The value  $dB\Omega$  is calculated as  $20[\log_{10}(Z_T/\Omega)]$ . The transimpedance gain is a complex quantity with frequency-dependent magnitude  $|Z_T(f)|$  and frequency-dependent phase shift  $\theta(f)$ . The transimpedance gain at low frequencies is usually flat, and represented by  $R_T$ . The first reason for having a TIA with high gain is to create a signal with amplitude large enough to drive the post amplifier. However, there is an additional reason, which might be even more important: noise. As the TIA is the first stage in the optical receiver, the noise of the next stages like the PA will be suppressed by the TIA gain. Therefore a lower transimpedance gain (for instance to obtain a higher bandwidth) cannot simply be exchanged for a larger post amplification [21].

Generally, the TIA output signal is still not large enough to reach detectable logic levels (a few hundreds mV<sub>pp</sub>) so additional amplification is added in the form of a limiting amplifier or AGC amplifier.

#### 3.2.1.2 Bandwidth and group delay

TIA bandwidth is defined as the frequency at which the transimpedance dropped by 3 dB below its midband value. The bandwidth of the optical receiver is usually determined by TIA [10]. It can be estimated by its  $RC$  time constant contributed by photodiode capacitance and total input capacitance and resistance of the amplifier circuit.

As mentioned above, practical TIAs contain multiple poles and zeros, requiring careful simulations to determine the eye closure and the jitter resulting from the

limited bandwidth. Even if the frequency response  $|Z_T(f)|$  is flat up to a sufficiently high frequency, distortions in the form of data-dependent jitter may occur if the phase linearity of  $Z_{TIA}(f)$  is insufficient. Therefore, the phase of  $Z_T(f)$  must be carefully simulated and linearity of the phase must be observed during the design as well. Variation of the *group delay* with frequency is a measure method for the phase linearity. The group delay,  $\tau$ , is related to the phase,  $\theta(f)$ , as [10].

$$\tau(\omega) = -\frac{d\theta}{d\omega} \quad (3.20)$$

The bandwidth and group delay variation are important parameters determining the amount of ISI and jitter introduced by the TIA. For 10 Gbit/s fiber optical speeds, the bandwidth required to prevent high amount of ISI corresponds to at least 7 GHz while group delay variation required to limit the generation of data-dependent jitter is  $|\Delta\tau| < 10 \text{ ps}$  [10].

### 3.2.1.3 Noise

The noise of the TIA mostly dominates all other noise sources (photodetector and post amplifier, etc) and therefore determines the sensitivity of the receiver. There are several noise definitions, which should be expressed before giving simulation results.

The input-referred noise current spectrum or power spectral density of the input-referred noise current  $\overline{i_{n,in}^2}(f)$  is one of the most critical TIA specifications. The input-referred noise current spectrum is the current source that, together with the ideal noiseless TIA, reproduces the output noise of the actual noisy TIA. It is a fictitious quantity that cannot be observed in the actual circuit [22]. As it will be seen in the following calculations and in the presented work, the input noise spectrum of TIA is not white. The power spectral density of the input-referred noise current is measured in  $\text{pA}^2/\text{Hz}$  and typically consists of a white part, an  $f^2$  part at high frequencies, and a  $1/f$  part at low frequencies (in fact, fiber communication rules does not allow such low frequencies). In addition to thermal noise of feedback resistor  $R_F$ , noise sources for the BJT typically are shot noises of collector and base currents, thermal noise of intrinsic base resistance. There are also flicker ( $1/f$  noise) and burst noise sources but they are not included in this project. The reason for this is that by the means of scrambling, low frequency component of the transmitted data is not allowed to be lower than a few ten kHz.

To determine the input-referred noise current spectrum, the noise power spectral density at the output for each noise source is calculated first. Assuming these sources are uncorrelated, they add up to form the output noise power spectral density  $\overline{v_{n,o}^2}$ . The power spectral density of the input-referred noise current  $\overline{i_{n,in}^2}$  can then be found by considering the frequency-dependent transimpedance gain:

$$\frac{\overline{i_{n,in}^2}}{\Delta f} = \frac{\overline{v_{n,o}^2}}{|Z_T(f)|^2} \quad (3.21)$$

The input-referred rms noise current or the total integrated input-referred noise current of the TIA  $\overline{i_{n,in,tot}}$  is determined by dividing the total integrated output noise voltage by the DC value of the transimpedance gain. The total output noise voltage  $\overline{v_{n,o,tot}}$  is obtained by integrating the output noise spectrum and taking the square root

$$\overline{v_{n,o,tot}} = \sqrt{\int_0^\infty \overline{v_{n,o}^2(f)} df} \quad (3.22)$$

$$\overline{i_{n,in,tot}} = \frac{\overline{v_{n,o,tot}}}{R_T} \quad (3.23)$$

For analytical calculations, the integration can be carried out to infinity [21]. However, for simulations and measurements, noise bandwidth equals to  $\pi/2$  times the  $-3dB$  bandwidth of a first order circuit [23].

Another noise definition is averaged input-referred noise current density  $\overline{i_{n,in,avg}}$ . This definition allows different TIAs having different bandwidth and gain to be compared because every design has different gain and bandwidth performance. Averaged input-referred noise current density can be found dividing the total input-referred current by square root of the  $-3dB$  bandwidth of the TIA.

$$\overline{i_{n,in,avg}} = \frac{\overline{i_{n,in,tot}}}{\sqrt{f_{-3dB}}} \quad (3.24)$$

#### 3.2.1.4 Wide input dynamic range

If transimpedance amplifier receives large input currents, they, like other analog circuits, introduce non-linearity in the signal as the input level increases. While the binary nature of the data may imply that a high non-linearity can be tolerated, other issues must be taken into account. Some TIA topologies or some types of transistors may distort the data waveform if the input current is large. For instance, bipolar devices in the signal path may enter saturation for one bit, failing to respond

properly to the next. Also, feedback circuits behave poorly if the signal drives the stages into saturation. Therefore, both high and low levels and zero crossings of waveforms may be corrupted. If maximum peak-to-peak input current is low, the problem of overload may mandate the use of automatic gain controller circuit [24]. This type of topology will increase the complexity of the circuits and power consumption will be higher [19].

### **3.2.1.5 Output impedance**

Apart from other requirements, when TIA is not integrated with the next stages, it must drive a 50-ohm transmission line on a printed-circuit board. In this case, the design will mandate inter-stage driver resulting in severe trade-offs between gain, power dissipation and bandwidth. CMOS and BiCMOS technologies are very attractive choice at this point. Especially, SiGe BiCMOS provides low noise and broadband solutions as well as providing integration with the next stages [25].

### **3.2.2 TIA circuit concepts**

Generally, there are two types of TIA topologies, open loop TIAs and feedback TIAs. The goal when designing a TIA is to provide a low input impedance in order to meet the bandwidth requirements while also providing low noise and high gain. Shunt-feedback TIA architecture is preferred in this project. However, before analyzing the shunt-feedback TIA, it will be instructive to start with basic transimpedance circuit. Figure 3.8 depicts basic current-to-voltage converter, in other words, transimpedance amplifier. Because photodiodes generates small current and since most of the subsequent process occurs in the voltage domain, the current must be converted to voltage. However, the time constraint  $R_C C_{in}$  leads to severe trade-off between gain, noise and bandwidth.

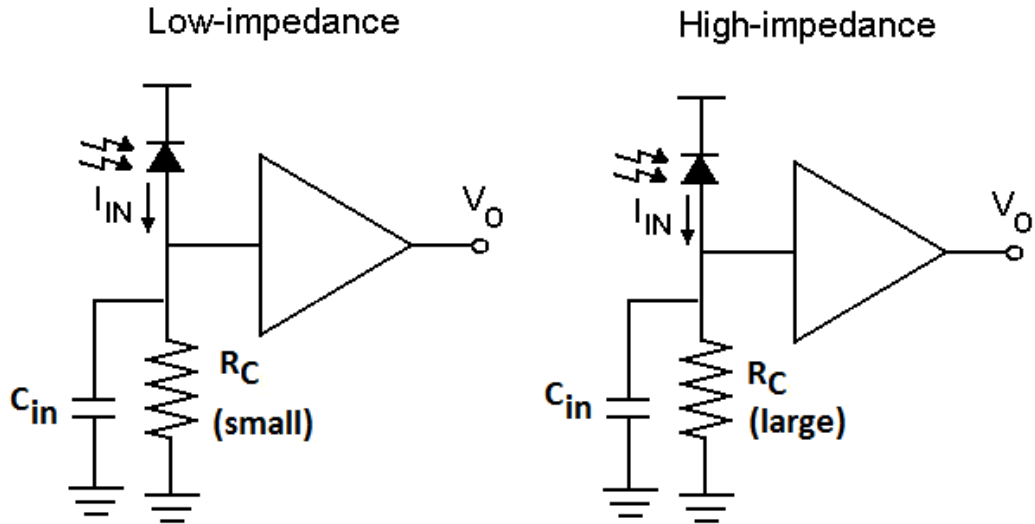


**Figure 3.8:** Low and high impedance TIA.

$C_{in}$  is the total capacitance (including photodiode capacitance) at the input node.  $R_C$  is the load resistor and equals to transimpedance gain  $R_T = R_C$ . The input-referred noise current spectrum is white and is given by the thermal noise of  $R_C$  in Equation (3.26). Bandwidth of the circuit can be written as

$$\omega_{3dB} = \frac{1}{R_C C_{in}} \quad (3.25)$$

$$\frac{\overline{i_n^2}}{\Delta f} = \frac{4kT}{R_C} \quad (3.26)$$

$R_C$  is typically  $50 \Omega$  in the case of low-impedance condition. One bottleneck is that  $R_C$  directly appears in both noise and bandwidth equations. The first drawback of this simple structure is that low transimpedance gain and therefore the small output voltage produced by this front-end for small input currents. Another drawback is the significant noise current associated with the small resistor value. However, the very first merit of the low-impedance front-end is large bandwidth due to the low  $R_C C_{in}$  time constant.

To get around the problems of the low-impedance front-end, high-impedance structure can be considered by increasing the load resistor  $R_C$ . The transimpedance increases compared to low-impedance TIA and the thermal noise is low due to high resistance. However, the price paid for increasing input resistance is that the bandwidth is reduced. An equalizer is needed to compensate the frequency response, which makes the amplifier design more complicated. Another drawback of the high-input impedance is voltage headroom will automatically drop because  $R_C$  also carries bias current. This basic example necessitates high performance

topologies and gives quick understanding about trade-offs between gain, noise, bandwidth and voltage headroom.

### 3.2.2.1 Open-loop TIA

Open-loop TIA with common-base (or common-gate) is better choice to get around the limited bandwidth caused by the large  $RC$  time constant at the input of the high-impedance TIA. A typical common-base TIA is depicted in Figure 3.9. The transistor  $T_1$  is the common-base transistor with a resistive load  $R_C$  while transistor  $T_2$  provides a bias current.

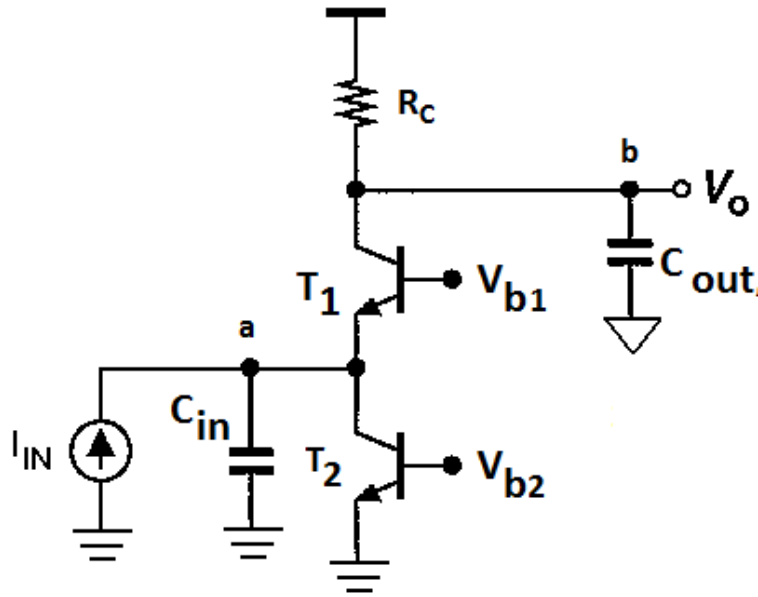


**Figure 3.9:** Typical open-loop TIA topology.

$C_{in}$  is the total input capacitance (photodiode capacitance, collector-base and collector-substrate capacitances of  $T_2$  and  $C_{\pi 1}$  of  $T_1$ ) at node  $a$ .  $C_{out}$  is the total output capacitance (input capacitance of subsequent stage, collector-base and collector-substrate capacitances of  $T_1$ ) at node  $b$ . To ease the transfer function calculations, the Early effect and base resistance are neglected. Under the condition  $\beta \gg 1$ , transfer function is

$$\frac{V_o}{I_{in}} = \frac{g_{m1}R_C}{(g_{m1} + sC_{in})(sR_C C_{out} + 1)} \quad (3.27)$$

In (3.27), transimpedance is approximately  $R_C$  while input impedance is about  $1/g_m$ . The low input resistance of the common-base stage helps to satisfy low input impedance at node  $a$ . Besides, common-base TIA isolates the photodetector capacitance (included in  $C_{in}$ ) from the critical node  $b$ . Therefore, decrease in input impedance at node  $a$  resulting in broadband operation giving more flexibility for gain,

bandwidth and noise trade-offs. However, for a given photodiode and technology, to improve bandwidth, collector current must be increased (to increase  $g_{m1}$ ). In this case, voltage drop across  $R_C$  will be higher, which degrades voltage headroom. Trying to reduce  $R_C$  will cause lower transimpedance and higher noise due to the thermal noise of  $R_C$ .

Total input-referred noise current can be extracted as in Equation (3.28) by neglecting  $C_{\pi1}$  and considering  $r_{b1}$  [19]

$$\overline{i_{n,in,tot}^2} = \frac{C_{in}(g_{m1}+2g_{m1}^2r_{b1})kT}{C_{out}R_C(C_{in}+g_{m1}R_C C_{out})} + \frac{kT}{C_{out}R_C^2} + \frac{2kTg_{m1}(g_{m1}+2/r_{b1})}{C_{in}+g_{m1}R_C C_{out}} \quad (3.28)$$

As performing current-mode operation, common-base (or common-gate) circuits are the first stage of the voltage amplifier [26], thereby degrading the noise performance. In (3.28), thermal noise of base resistance appears directly along with the collector current shot noise. Larger transistors will have smaller base resistance but, in this case, junction capacitances will be higher [19]. Thus, this architecture contributes extra noise to the overall TIA. The load resistor (and transimpedance)  $R_C$  again carries the bias current thereby trading with noise and voltage headroom.

### 3.2.2.2 Feedback TIA

The most commonly employed circuit topology for preamplifiers in optical fiber applications is shunt-feedback transimpedance amplifier shown in Figure 3.10. The tight trade-offs in common-base circuits make it difficult to achieve low noise and low power operation. As mentioned above, the noise current of the load resistor and the biasing transistor (could be resistor as well) are directly referred to the input, leading to a high noise at low supply voltage [19]. To overcome these issues, shunt-feedback amplifier, which is a current-to-voltage converter with a negative resistive feedback, is chosen in this design because it provides a large bandwidth by synthesizing a small input-impedance while maintaining a large resistor value in the feedback path to improve noise behavior.

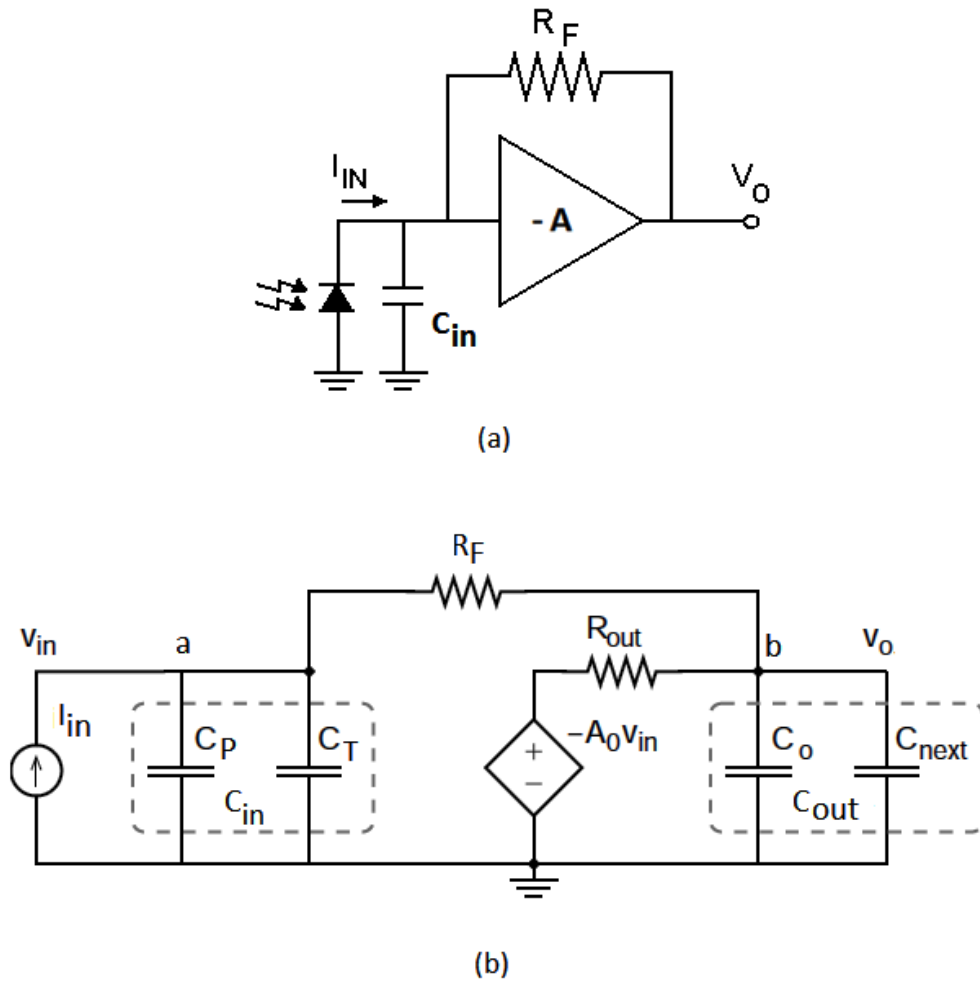


**Figure 3.10:** Second-order feedback transimpedance amplifier with small-signal equivalent.

Feedback transimpedance amplifier is a popular approach to avoid the dynamic range problem because  $R_F$  feedback resistor does not have to carry bias current. In this topology, negative feedback network senses the voltage at the output and returns a proportional current to the input. This type of feedback is chosen because firstly, it lowers the input resistance thus increasing the input pole magnitude and allowing amplifier bandwidth to be higher. Secondly, the feedback structure also reduces output resistance thereby yielding better drive capability [21].

Since the presented design is realized in this topology, performance specification of the feedback transimpedance amplifier is deeply investigated. In Figure 3.10, core amplifier is modeled with single pole and small-signal equivalent is depicted at the bottom. By assuming that voltage amplifier has one pole, overall TIA becomes second-order. Transfer function of voltage amplifier can be modeled as

$$A(s) = \frac{A_0}{1+s/\omega_0} \quad (3.29)$$

Where  $A_0$  is the DC voltage gain and  $\omega_0 = 1/R_{out} C_{out}$ . For  $A_0 \gg 1$  the transfer function can be obtained as

$$\frac{V_{out}}{I_{in}} = -\frac{R_F A_0}{\frac{R_F C_{in}}{\omega_0} s^2 + \left(R_F C_{in} + \frac{1}{\omega_0}\right) s + A_0 + 1} \quad (3.30)$$

From the Equation (3.30), DC transimpedance gain equals to  $R_T \approx R_F$

The two poles of a second-order system are mostly part of a complex conjugated pair. In basic control theory, the denominator of a second-order system is given as [27]

$$\left(\frac{s}{\omega_n}\right)^2 + 2\zeta\left(\frac{s}{\omega_n}\right) + 1 \quad (3.31)$$

Where  $\zeta$  is the dimensionless damping ratio and  $\omega_n$  is the natural pulsation of the system. When  $\zeta = 1$ , the system is critically damped. Complex conjugated poles occur. Smaller  $\zeta$  will result in a larger -3dB bandwidth, but also a higher overshoot in the time domain and a larger resonance peaking in the frequency domain. That being the case, even if smaller  $\zeta$  means a larger bandwidth, it may degrade eye opening and jitter performance in the eye diagrams [21]. In [27], the percent overshoot  $PO$  is

$$PO = 100e^{-\zeta\pi/\sqrt{1-\zeta^2}} \quad (3.32)$$

When  $\zeta=\sqrt{2}/2$ , which corresponds to Butterworth response, maximally flat frequency response is obtained. This leads to 4 % overshoot with phase margin  $45^\circ$ . In the case of  $\zeta=\sqrt{3}/2$ , which corresponds Bessel response, maximally flat phase response (small group delay variation) is gathered. Bessel response uses a rather safe phase margin of at least  $72^\circ$  with the overshoot of 0.4 % in the time domain.

If at least 8-9 GHz bandwidth is somehow achieved, then Bessel design will be a good choice to achieve very good eye openings at the output. Furthermore, by providing additional margin, secondary effects such as parasitic capacitances, temperature and process variations can be compensated for during the chip design.

Equating (3.31) with the denominator of (3.30) yields the following results:

$$\omega_n^2 = \frac{\omega_0(A_0+1)}{R_F C_{in}} \quad (3.33)$$

$$\zeta = \frac{1}{2} \frac{R_F C_{in} \omega_0 + 1}{\sqrt{(A_0 + 1) \omega_0 R_F C_{in}}} \quad (3.34)$$

To get Bessel response, damping ratio equals to  $\zeta = \sqrt{3}/2$ . In this case, natural pulsation and bandwidth is

$$\omega_n = \frac{\sqrt{3} A_0}{R_F C_{in}} \quad (3.35)$$

$$\omega_{3dB} = \frac{1.07 A_0}{R_F C_{in}} \quad (3.36)$$

The dominant pole, which determines the bandwidth, is located at the input node (node *a*) of voltage amplifier. Due to the feedback loop, the resistance at the input node is divided by the loop gain, which results in a factor of  $1.07A_0$  increase in bandwidth. Bandwidth is increased because the pole introduced by the core amplifier creates an inductive behavior in the input impedance of the TIA, partially cancelling the roll-off due to the input capacitance [19]. A design aiming for high bandwidth implies an optimization of the voltage gain  $A_0$ . Therefore,  $A_0$  has to be maximized during the design process, which is mostly related to technology. Other factors that influence bandwidth are the feedback resistor  $R_F$  and the total input capacitance  $C_{in}$ .  $R_F$  usually cannot be made too small for gain and noise considerations.  $C_{in}$  consists of two parts:  $C_P$ , determined by the photodiode topology, and  $C_T$ , which increases for larger transistor dimensions. The non-dominant pole is located at the output node. It coincides with the bandwidth of the voltage amplifier, which has only one pole in the simplified model of Figure 3.9.

Equation (3.36) reveals one important conclusion: As the total input capacitance is largely determined by the photodiode capacitance, whose parameters are dictated by technology rules and fiber size,  $A_0$  is the critical parameter to obtain higher gain and bandwidth.

As it will be stated in the following, noise can be very low due to large feedback resistance. One problem to be careful about is the stability that comes with the feedback technique. However, in this design, it has been tried to get around the stability issue by producing Bessel response, which has relatively large phase margin.

### Shunt-feedback TIA noise calculations

The noise that affects the sensitivity is primarily related to the transimpedance input impedance. Input impedance is determined mostly by the photodetector capacitance, and hence this capacitance must be specified when quoting the input-referred noise current.

Figure 3.11 illustrates typical noise contributions of a BJT implemented feedback TIA. One is the thermal noise of the feedback resistor  $i_{n,RF}$ . The bipolar front-end produces shot noise due to the base current,  $i_{n,B}$ , thermal noise due to the intrinsic base resistance,  $i_{n,rb}$ , and shot noise due to the collector current,  $i_{n,C}$ . The effect of all these noise sources can be described by a single equivalent noise current source  $\overline{i_{n,in}^2}$  at the input of the TIA. In differential circuits, noise contribution of the other symmetric components must be taken into account.

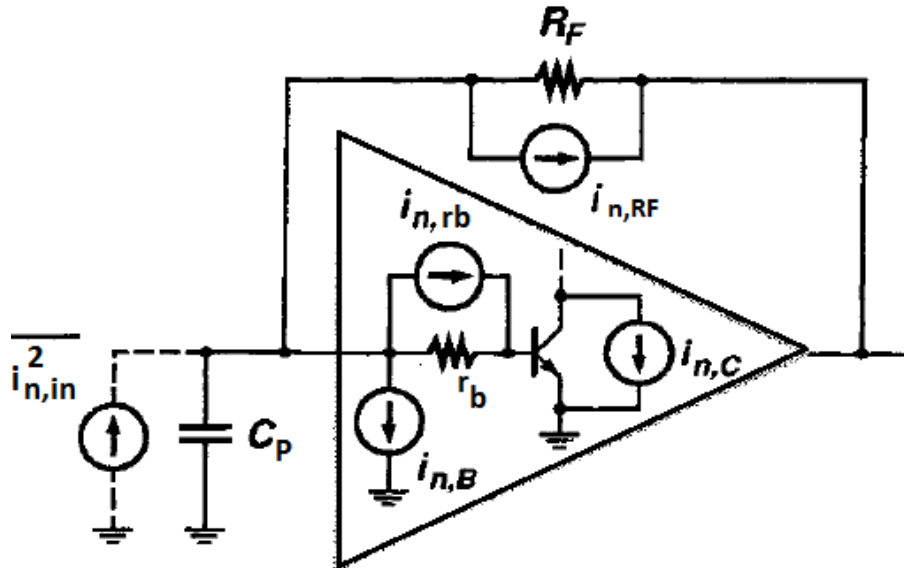


Figure 3.11: Noise contributions in feedback TIA.

The input-referred noise current spectrum of the TIA can be broken into two major components: the noise from the feedback resistor and the noise from the amplifier front-end. They all can be defined as

$$\frac{\overline{i_{n,RF}^2}}{\Delta f} = \frac{4kT}{R_F} \quad (3.37)$$

$$\frac{\overline{i_{n,B}^2}}{\Delta f} = 2qI_B \quad (3.38)$$

$$\frac{\overline{i_{n,C}^2}}{\Delta f} = 2qI_C \quad (3.39)$$

$$\frac{\overline{i_{n,rb}^2}}{\Delta f} = \frac{4kT}{r_b} \quad (3.40)$$

In high-speed receivers, front-end noise contribution is typically larger than the contribution from the feedback resistor. However, in low-speed receivers, the resistor noise may become dominant [21]. The noise current spectrum of the feedback resistor is white frequency-independent and given by the well-known thermal noise equation. This white noise current contributes directly to the input-referred noise current of TIA. Because noise sources are uncorrelated, input-referred noise current spectrum can be approximated as [10, 22]

$$\frac{\overline{i_{n,in}^2(f)}}{\Delta f} = \frac{4kT}{R_F} + \frac{2qI_C}{\beta} + \frac{2qI_C}{g_m^2 R_F^2} + 2qI_C \frac{(2\pi C_T)^2}{g_m^2} f^2 + 4kT r_b (2\pi C_P)^2 f^2 \quad (3.41)$$

Where  $C_T$  is the total capacitance at the input of the BJT. Equation (3.41) reveals important noise results. Input-referred noise current spectrum  $\overline{i_{n,in}^2}$  consists of mostly white noise terms and  $f^2$  terms. It is worth to say that white shot noise transforms to frequency dependent  $f^2$  noise. Photodiode capacitance as being source capacitance directly appears with  $f^2$  part. It will be effective at high frequencies degrading the sensitivity. Since it decreases the susceptance at high frequencies and improves the noise matching, coupling the photodetector with a small inductor is a popular method [28]. The fifth term increases with the intrinsic base resistance  $r_b$  and can be minimized through layout considerations or by choosing a technology having low  $r_b$  such as SiGe heterojunction bipolar transistor technology.

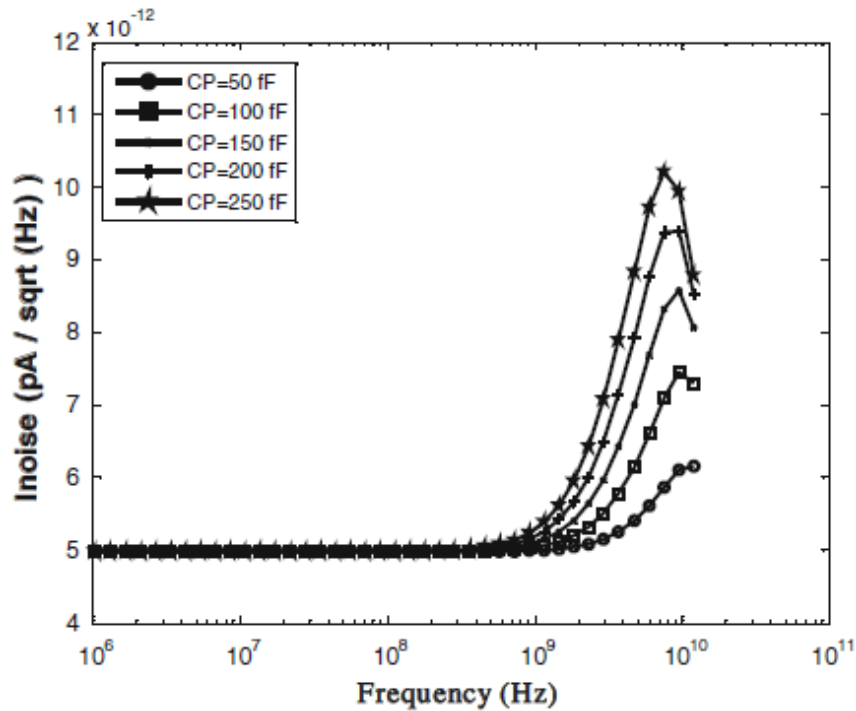


**Figure 3.12:** Photodiode capacitance,  $C_p$ , effect on noise performance of TIA.

Figure 3.12 depicts the Equation (3.41). As stated above, photodiode capacitance,  $C_p$ , directly affects noise performance of the TIA. In this case,  $C_p$  is swept from 50 fF to the 250 fF. As  $C_p$  becomes higher, noise of the circuit increases for the same operating frequency after around 1 GHz. It can be seen from the plot that low frequency noise sources of BJT do not appear even at the frequencies around 1 MHz.

### 3.2.2.3 Differential TIA

Single-ended architectures, despite the advantages of low-noise and low-power consumption, are not suitable because they are very susceptible to supply noise and are prone to stability problems stemming from parasitic feedback paths. A large substrate cross-talk noise, when integrated with other digital circuits, may also significantly deteriorate the performance of a receiver [19]. The primary methods used to alleviate the large supply noise present in a mixed digital and analog circuit environment are to keep the sensitive analog parts away from the noisy digital parts, or to block the noise transmission from the digital circuits [29, 30]. Thus, in addition to careful layouts including separate power supply lines and shields, differential circuit architectures are inevitable in designing TIAs that are susceptible to substrate noise [29, 30]. Differential TIAs attempt to remove noise from their inputs by using

parallel signal paths. Differential TIAs are, however, noisier than the same single-ended ones. The input-referred noise power is twice that given in Equation (3.41).

The other bottleneck of differential TIA is that photodiode produces a single-ended current leading several difficulties. Figure 3.13 illustrates differential shunt-feedback TIA. To alleviate this condition and to get around the asymmetry problems, some techniques are implied in the next section such as replicating the photodiode capacitance at the unused input.

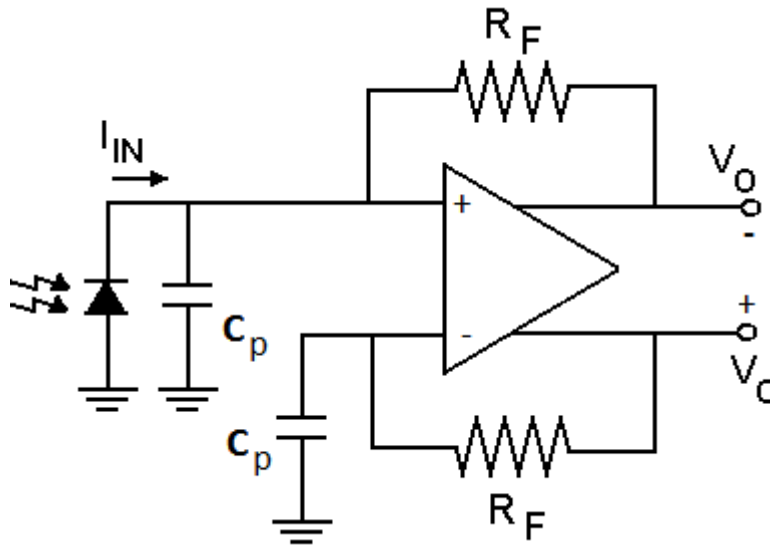


**Figure 3.13:** Differential TIA with replicated capacitance.

### 3.3 Silicon-Germanium Heterojunction Transistors

Very high bandwidth and low-noise TIAs are needed for 10 Gbit/s fiber optical receivers. Semiconductor devices having relatively high  $f_T$  therefore must be incorporated in these applications. Until recent years, high-cost III-V semiconductor technologies, such as GaAs and InP, have dominated the optical front-ends and receivers [31, 32] because they exhibited excellent performance in speed and noise. These technologies also exhibit high junction breakdown voltage which is not strictly necessary for TIAs because the output swing of the fiber optical amplifiers is usually lower than 1 V. Silicon based bipolar TIAs were also presented. The major demerit of the Si-bipolar TIAs was that they generally showed poor noise performance and lower sensitivity [33]. CMOS process is also becoming a low cost, low power choice for lower data rates [34]. Bipolar transistors, however, are faster than CMOS transistors for the same size and higher transconductance can be achieved. SiGe heterojunction bipolar technology has recently provided a cost-effective alternative

and higher integration levels, especially SiGe BiCMOS process, with improved sensitivity for 10-Gbit/s fiber optical front-ends and for the development of photoreceivers. One of the most important advantages of the SiGe BiCMOS technology is that it enables analog and digital parts of the optical receiver to be integrated in the same chip. In that case, output drivers and output impedance matching networks are avoided. Since SiGe simultaneously enables high speed and low power consumption, it has been becoming an important choice for the realization of high speed fiber optical receivers.

SiGe BiCMOS applications range from wired and wireless communications circuits, to disk storages, to high speed, high bandwidth instrumentation. The usage of discrete SiGe HBTs and amplifiers in wireless devices is common place. In addition to highly occupation in high speed 10-40 Gbit/s optical receivers, integrated BiCMOS SiGe chips can be found in GSM, wireless LAN chipsets etc.

The concept of combining Silicon (Si) and Germanium (Ge) into an alloy for usage in transistor engineering is an old one. However, because of difficulties in growing lattice-matched SiGe alloy on Si, this concept is reduced to practical reality only in the last 25 years [35]. SiGe HBT technology was originally developed at IBM. However, that effort failed to CMOS, primarily because of its high power consumption [35]. Figure 3.14 illustrates two base contacts NPN SiGe cross-section.

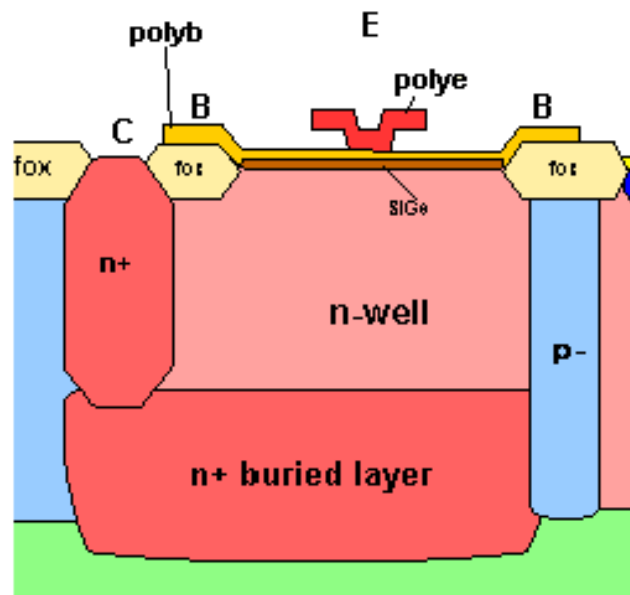


**Figure 3.14:** Cross-section of vertical NPN SiGe transistor.

A SiGe HBT is similar to a conventional Si bipolar transistor except for the base. SiGe, a material with narrower bandgap than Si, is used as the base material. Ge composition is typically graded across the base to create an accelerating electric field for minority carriers moving across the base [36-40].

A direct result of the Ge grading in the base is higher speed, and thus higher operating frequency. The transistor gain is also increased compared to a Si BJT, which can then be traded for a lower base resistance, and hence lower noise. For the same amount of operating current, SiGe HBT has a higher gain, lower RF noise, and low  $1/f$  noise than an identically constructed Si BJT [36]. The higher raw speed can be traded for lower power consumption as well. One major drawback of the SiGe is low junction break-down voltages. This specification limits the design flexibility as given in the next section.

As stated above, the real strength of SiGe lies in its ability to integrate analog, RF and digital architectures on a single package using existing CMOS fabs. This is not possible with any other technologies such as GaAs etc [35].

## 4. DESIGN OF DIFFERENTIAL TRANSIMPEDANCE AMPLIFIER IN SiGe BiCMOS FOR 10 Gbit/s FIBER OPTICAL RECEIVERS

This chapter presents a differential, low-noise transimpedance amplifier for 10 Gbit/s fiber links using AMS 0.35  $\mu\text{m}$  SiGe HBT BiCMOS process, which is suitable for 10 Gbit/s photoreceivers. Circuit is realized in the ITU VLSI Laboratories using the Cadence Design Environment tool.

At the beginning of the circuit design, transistors in the signal path are searched for highest  $f_T$ . At the collector current between 0.4-0.62 mA, the 12  $\mu\text{m}$  length and 0.4  $\mu\text{m}$  width emitter size SiGe exhibited largest  $f_T$  (for the 2 base contacts vertical SiGe). However, this result helped only to pay more attention to the dimensions and bias currents. To get very good performance results, the emitter size of the transistors (together with the other parameters for sure) were varied around these dimensions. All components and parameters in the realized TIA are implemented in RF models.

Apart from TIA design requirements widely discussed in the previous section, the two major bottlenecks were avoided: First, BJTs had not to go into saturation region even at highest input currents. Second, it had to be cared about low breakdown voltages of junctions, which is 1 V for the base-emitter junction and 2 V for the collector-emitter junction.

### 4.1 Circuit Design

As a first stage, TIA must have a very little group delay deviation from the low frequencies up to high frequencies because time jitter caused by excessive group delay variation cannot be compensated for at the succeeding stages. In contrast, a drop in signal magnitude at higher frequencies can be improved by using PA after the TIA. That being the case, lowering the group delay variation over the bandwidth was one of the major issues during the design. This issue is mostly overcome by obtaining and realizing Bessel type TIA. The advantage of Bessel response was indicated in section three.

Figure 4.1 illustrates eye diagrams of Butterworth and Bessel TIAs. In this example, NRZ of 10 Gbit/s PRBS signal is applied to the input of Butterworth and Bessel TIA

having 6 GHz bandwidth. As it is seen from the Figure 4.1, even with a bandwidth at almost half the speed of the input signal, the Bessel TIA still has an open eye, compared to that for a Butterworth TIA. The nature of the Bessel transfer function makes it relatively immune to parasitic that can cause ringing. This is an advantage for integrated circuit design, where the circuit parameters of the fabricated chip vary from the ideal layout simulation.

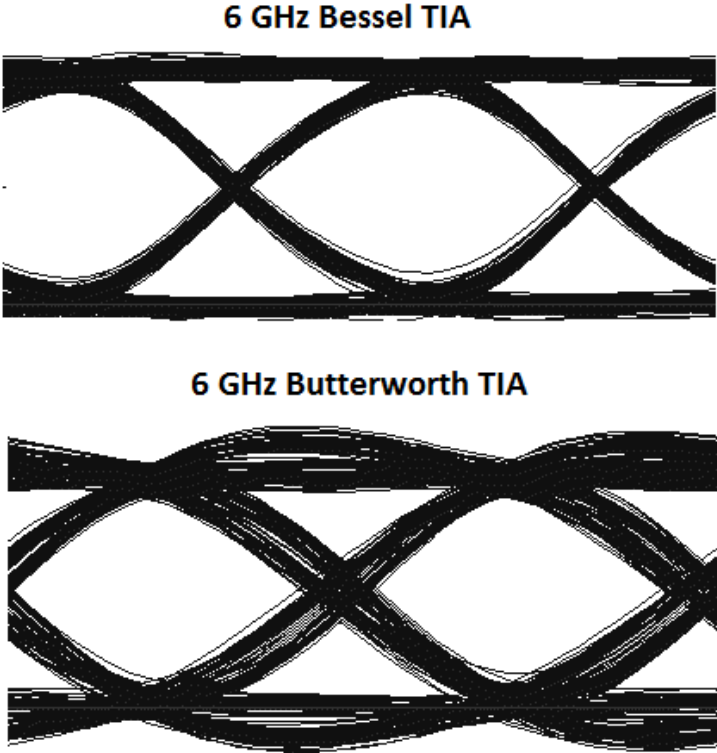


**Figure 4.1:** Result of limited bandwidth on Bessel and Butterworth TIAs.

Since post amplifier is differential, the circuit satisfying differential operation must be built. For single-ended output TIA, this might be done by applying reference voltage to the one input of the PA and applying TIA output to the other input [41]. This technique requires design of reference voltage generator. In other case, TIA can be realized in differential architecture having differential outputs. The latter makes the TIA immune to any common mode noise that it is preferred over the single-ended structure. As stated before, however, the input-referred noise power of the differential TIA is twice than that of the single-ended structure.

Cascode [42] and inductive peaking [43] techniques including active inductive peaking [44] were the alternative choices to reach the desired bandwidth of the transimpedance amplifier (around 8-9 GHz). Broadband operation, however, has been succeeded without using these techniques. Common-emitter with shunt-

feedback resistor is included in the circuit because of its good performance over the common-base structure, particularly in noise, dynamic range and low power consumption.

Realized differential SiGe TIA schematic is shown in Figure 4.2. The PIN photodiode with the intrinsic capacitance of 100 fF is modeled at the input of the circuit. Since photodiode output is single-ended, current from the photodiode is directed to the only one input of the TIA ( $T_1$ ). In this case, photodiode capacitance  $C_P$  is replicated at the other input ( $T_2$ ) to achieve fully symmetrical operation. This can be accomplished during chip design by placing dummy photodiode to the unused input of  $T_2$ . Alternatively, by the help of the knowledge of the total capacitance (including parasitic capacitances and if exists bond wire inductance) at the input of  $T_1$ , the same total impedance can be placed to the other input of the TIA [45]. The dominant pole of the differential TIA is defined by the time constant at the input node. Shunt-feedback resistors  $R_F$  are applied around voltage amplifier to reduce input impedance, which also reduces time constant at the input nodes allowing -3dB cut-off frequency to be higher. Emitter followers ( $T_3$ ,  $T_4$ ,  $T_5$  and  $T_6$ ) are used for DC level shifting and as buffer to drive next stages. The outputs are isolated from the feedback networks in order to prevent transimpedance gain and bandwidth from degradation because of the loading effect of the subsequent stage. Current mirrors are incorporated in the circuit as loads in order to neglect high value resistors from the circuit. All diode-connected transistors are needed for level shifting in order to keep  $V_{CE}$  less than breakdown voltage. Beta helper ( $T_8$ ) and emitter degeneration resistors are used at the biasing circuit in order to improve current matching performance of the current mirrors.

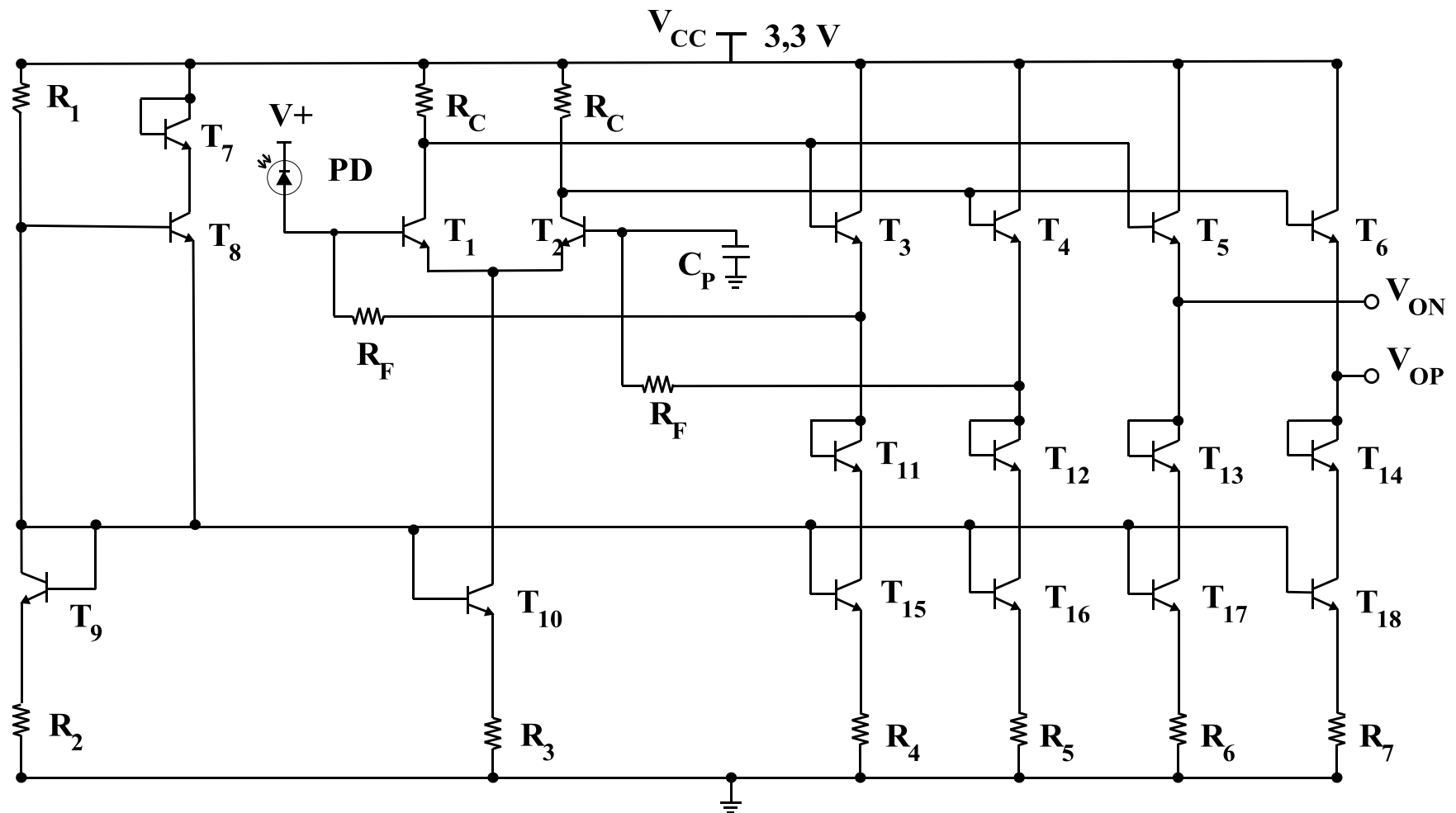
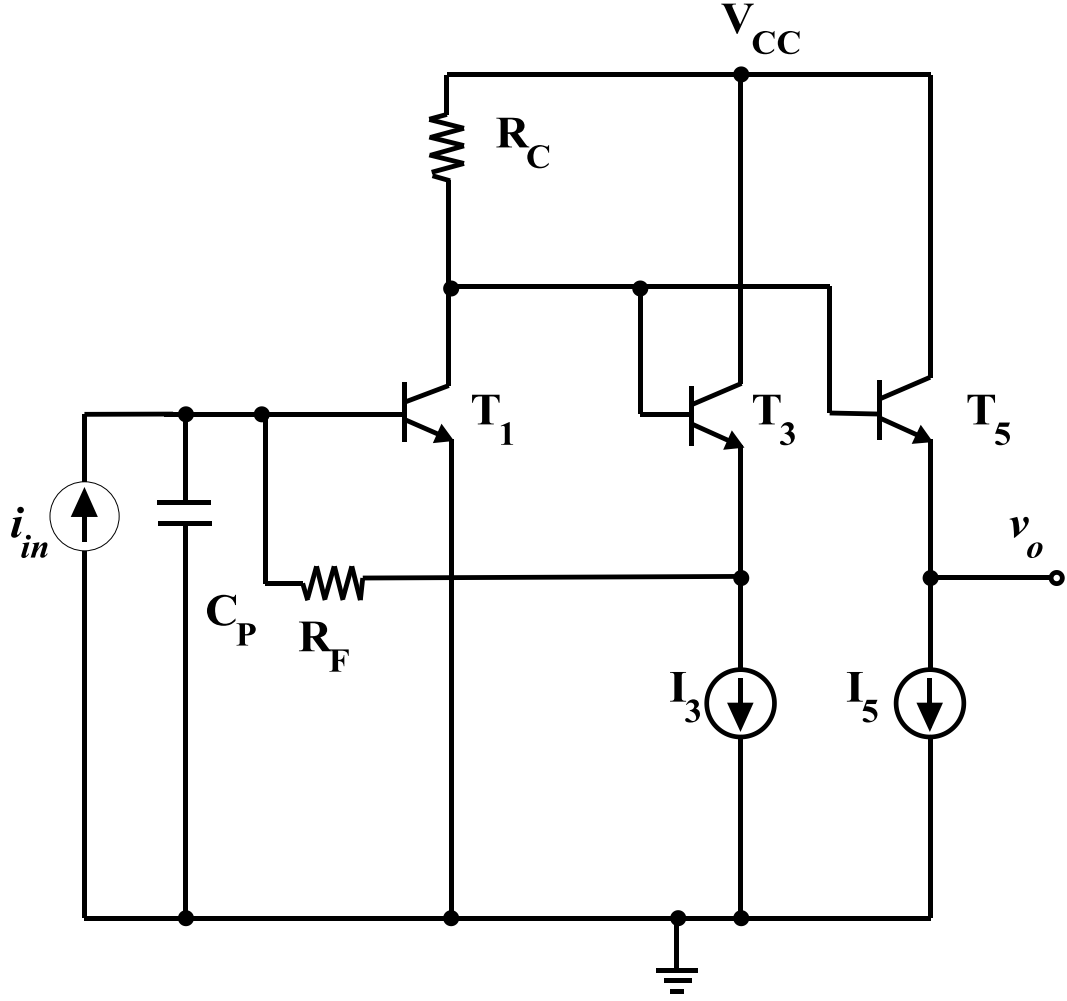


Figure 4.2: Realized differential SiGe TIA schematic.



**Figure 4.3:** Half-circuit model of the differential SiGe TIA with photodiode small-signal model.

To extract transfer function and noise equations, half-circuit model of the differential TIA is used shown in Figure 4.3. The TIA has a voltage amplifier and a shunt-feedback resistor  $R_F$ .  $I_3$  and  $I_5$  are the current sources representing the current mirrors. Voltage gain of the emitter follower at the last stage is assumed approximately one.  $T_1$  and  $T_3$  are accepted as the same transistors. Voltage amplifier is modeled with a single dominant pole. With the help of [10, 21, 46] transimpedance  $Z_T$  is

$$Z_T(s) = -\frac{A_o R_{eff}}{1 + s \frac{R_{eff}}{R_F} (\tau_c + C_t R_F') + s^2 \tau_c C_t R_{eff}} \quad (4.1)$$

where

$$A_o = -g_m R_c \frac{r_\pi}{r_b + r_\pi} \quad (4.2)$$

$$R_{eff} = \frac{r_{\pi} R_F}{r_{\pi}(1 + A_o) + R_F} \quad (4.3)$$

$$C_t = C_p + C_{\pi} + C_{\mu}(1 + A_o) \quad (4.4)$$

$$\tau_c = R_c(2C_{\mu} + C_{cs}) \quad (4.5)$$

$$R_F' = \frac{R_F r_{\pi}}{R_F + r_{\pi}} \quad (4.6)$$

Where  $C_{\mu}$  is the base-collector capacitance;  $C_{cs}$  is the collector-substrate capacitance and  $C_t$  is the total capacitance at the input of the TIA.  $r_b$  is the intrinsic base resistance;  $r_{\pi}$  and  $C_{\pi}$  base-emitter resistance and capacitance, respectively.  $A_o$  is the open loop DC voltage gain. From (4.1), DC transimpedance gain  $R_T$  is

$$R_T = \frac{v_o}{i_{in}} = -A_o R_{eff} \quad (4.7)$$

In a second order system, the damping factor must be equal to  $\frac{\sqrt{3}}{2}$  in order to obtain Bessel response which has a maximally flat group delay in the pass band. Using  $\frac{\sqrt{3}}{2}$  in Equation (4.1), bandwidth of the TIA is

$$f_{-3dB} = \frac{1.07 A_o}{2\pi R_{eff} C_t} \quad (4.8)$$

This result mandates that bandwidth of the voltage amplifier must be a factor 3 larger than the unity-gain frequency of the open-loop response [21]. Since, input transistors  $T_1$  and  $T_2$  are biased for highest  $f_T$ ,  $R_c$  and  $R_F$  are the major design parameters to obtain maximally linear phase response.  $R_F$  is also restricted by the transimpedance gain and noise parameters. Since input impedance directly affects stability of the TIA, HBT with 2 base contacts are chosen in order to make a compromise between base resistance and base parasitic capacitance.  $R_c$  and  $R_F$  are chosen as 900  $\Omega$  and 150  $\Omega$ , respectively. All circuit device values including emitter sizes of transistors are provided in Table 4.1. Emitter width is fixed to 0.4  $\mu\text{m}$  for all HBTs and lengths are changed for the needed size. Table 4.2 gives DC operating points of the transistors in the signal path. Small breakdown voltage of collector-emitter junction is avoided even at the maximum input levels. Transient node voltages are not more than 1.9 V when the input current is 400  $\mu\text{A}_{pp}$ .

**Table 4.1:** Device values and transistor emitter sizes.

$R_F$ 900 $\Omega$	$R_C$ 150 $\Omega$	$R_1$ 830 $\Omega$	$R_2$ 100 $\Omega$	$R_3$ 15 $\Omega$	$R_4$ 40 $\Omega$	$R_5$ 40 $\Omega$	$R_6$ 40 $\Omega$	$R_7$ 40 $\Omega$	$C_P$ 100 fF
Emitter Size									
$T_1$ 2.4 $\mu\text{m}^2$	$T_2$ 2.4 $\mu\text{m}^2$	$T_3$ 4.8 $\mu\text{m}^2$	$T_4$ 4.8 $\mu\text{m}^2$	$T_5$ 4.8 $\mu\text{m}^2$	$T_6$ 4.8 $\mu\text{m}^2$	$T_7$ 4.8 $\mu\text{m}^2$	$T_8$ 9.6 $\mu\text{m}^2$	$T_9$ 9.6 $\mu\text{m}^2$	
$T_{10}$ 2.4 $\mu\text{m}^2$	$T_{11}$ 4.8 $\mu\text{m}^2$	$T_{12}$ 4.8 $\mu\text{m}^2$	$T_{13}$ 4.8 $\mu\text{m}^2$	$T_{14}$ 4.8 $\mu\text{m}^2$	$T_{15}$ 4.8 $\mu\text{m}^2$	$T_{16}$ 4.8 $\mu\text{m}^2$	$T_{17}$ 4.8 $\mu\text{m}^2$	$T_{18}$ 4.8 $\mu\text{m}^2$	

**Table 4.2:** Transistor biasing points.

$T_{10}$	$T_1$	$T_2$	$T_3$	$T_4$	$T_5$	$T_6$
$I_C=5.6$ mA	$I_C=2.8$ mA	$I_C=2.8$ mA	$I_C=3.58$ mA	$I_C=3.58$ mA	$I_C=3.57$ mA	$I_C=3.57$ mA
$V_{CE}=1.048$ V	$V_{CE}=1.736$ V	$V_{CE}=1.736$ V	$V_{CE}=1.283$ V	$V_{CE}=1.283$ V	$V_{CE}=1.048$ V	$V_{CE}=1.048$ V

Equivalent input-referred noise current spectrum  $\overline{i_{n,in}^2}$  of the half-circuit can be written as;

$$\overline{i_{n,in}^2} = \frac{4KT}{R_F} + 4KT r_b |sC_p|^2 + 2q \frac{I_{C1}}{\beta} + \frac{1}{g_{m1}^2 |Z_{\pi1}|^2} \left[ 2qI_{C1} + \frac{4KT}{R_c} + \frac{v_{n3}^2}{\Delta f} \frac{1}{R_c^2} + \frac{v_{n5}^2}{\Delta f} \frac{1}{R_c^2} \right] \quad (4.9)$$

Where

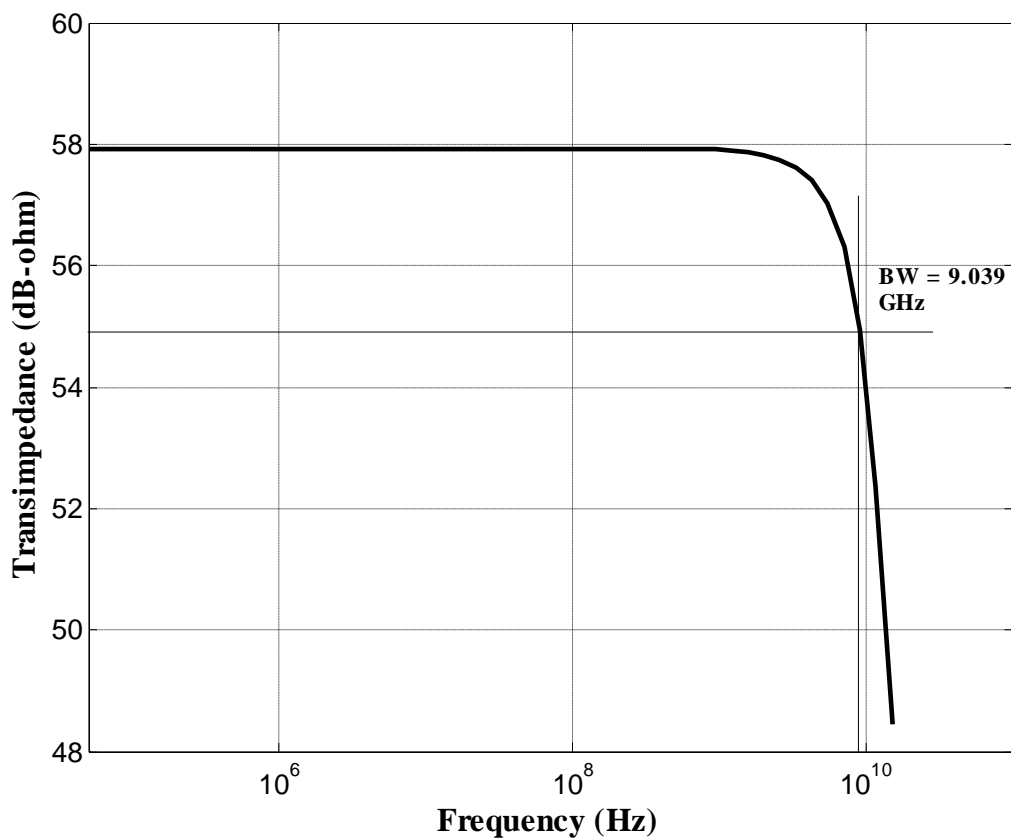
$$\frac{v_{n5}^2}{\Delta f} = 2qI_{C5} |Z_{e5}|^2 + 2qI_{B5} \left| \frac{1}{sC_{\mu4}} // Z_{\pi5} \right|^2 + 4KT r_b \quad (4.10)$$

$$\frac{v_{n3}^2}{\Delta f} = 2qI_{C3} |Z_{e3} // R_F|^2 + 2qI_{B3} \left| \frac{1}{sC_{\mu3}} // Z_{\pi3} \right|^2 + 4KT (r_b + R_F) \quad (4.11)$$

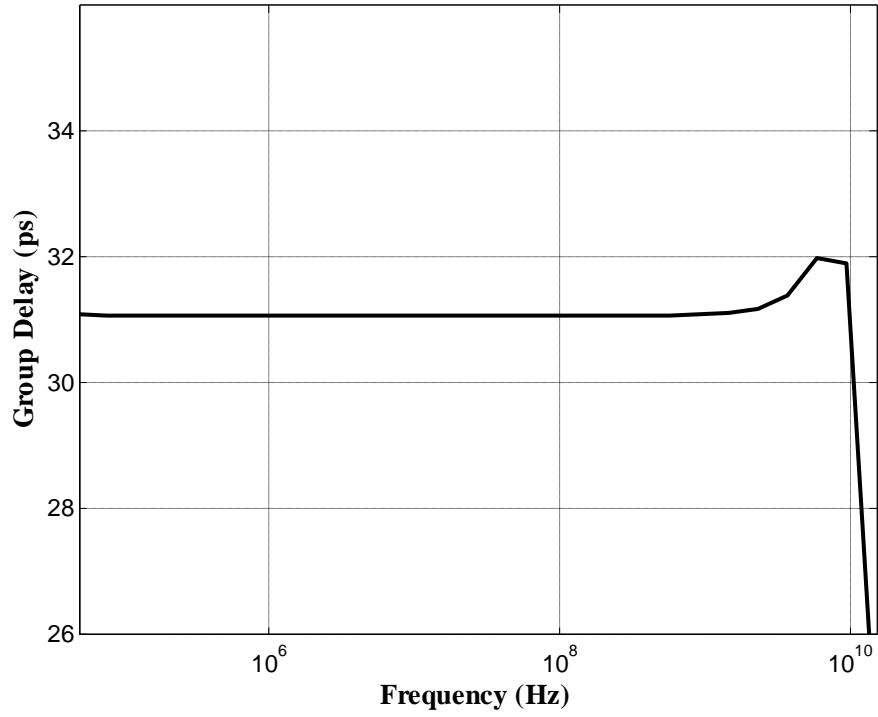
$k$  is the Boltzmann constant,  $T$  is the temperature in Kelvin and  $q$  is the electric charge.  $\overline{v_{n3}^2}$  and  $\overline{v_{n5}^2}$  are the equivalent input-referred noise voltage generators at the input of the  $T_3$  and  $T_5$ , respectively. For entire circuit  $\overline{i_{n,in}^2}$  is twice that given in Equation (4.9). Dominant noise sources are base and collector shot noise sources of the input transistors  $T_1$  and  $T_2$  (3<sup>rd</sup> and 4<sup>th</sup> terms in Equation (4.9)) and thermal noise sources from  $R_F$  feedback resistors and intrinsic base resistances  $r_b$  (first and second terms in Equation (4.9)). Since low frequency corner of fiber communications is a couple of kHz, flicker and burst noise sources are neglected.

## 4.2. Simulation Results

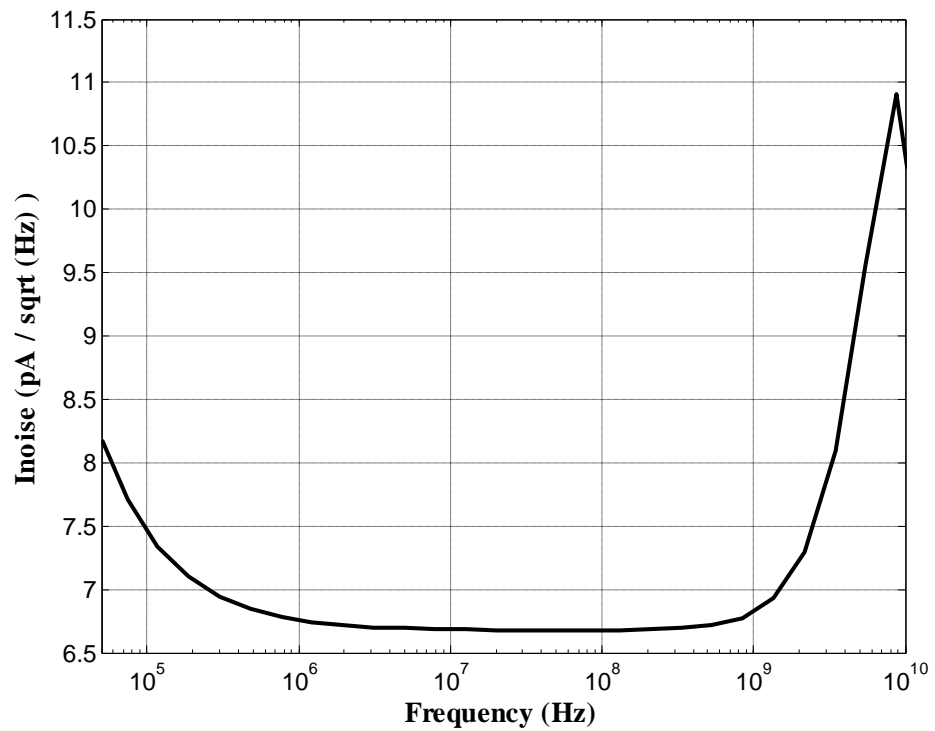
Simulation is performed by using the technology of  $0.35\mu$  SiGe HBT BiCMOS process whose  $f_T$  is about 70 GHz. Figure 4.4 shows differential transimpedance gain of the SiGe TIA. Flat frequency response is achieved. Bandwidth is 9 GHz and low frequency differential transimpedance gain is  $57.93\text{ dB}\Omega$  (making  $800\ \Omega$  which is almost equal to  $R_F$ ). Figure 4.5 depicts group delay variation over the frequency. Less than 1 ps change over the bandwidth is succeeded. These results coincide with the theoretical calculations given above.



**Figure 4.4:** Differential transimpedance gain of the TIA.



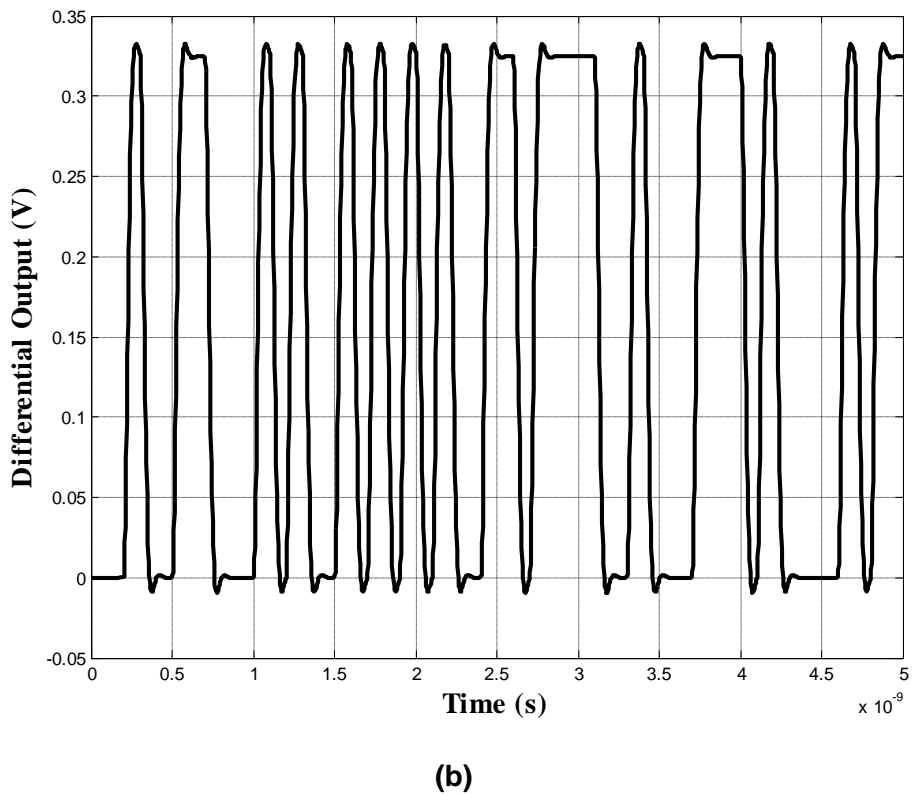
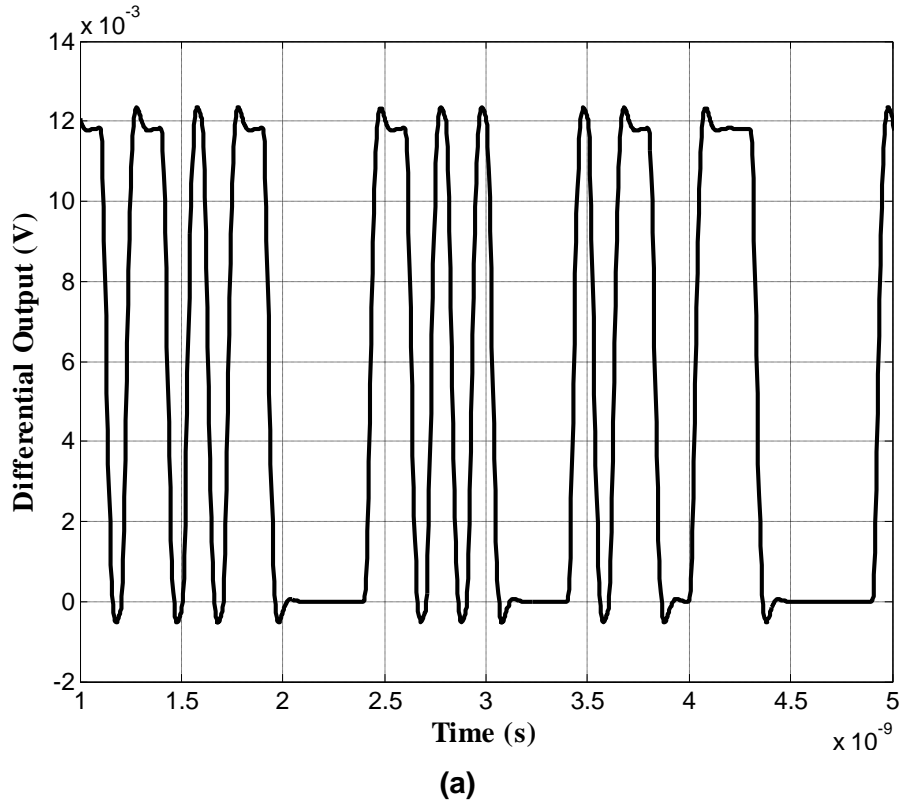
**Figure 4.5:** Group delay variation of the frequency response over the bandwidth.



**Figure 4.6:** Total input-referred noise current spectrum of the differential TIA.

Input-referred noise current spectrum is illustrated in Figure 4.6. Noise current is below  $7 \text{ pA}/\sqrt{\text{Hz}}$  up to 1 GHz. It is less than  $11 \text{ pA}/\sqrt{\text{Hz}}$  between 1 GHz and 9 GHz. Total integrated input-referred noise current  $\overline{i_{n,in,tot}}$  is  $1.061 \text{ } \mu\text{A}$ . 15 GHz noise bandwidth is considered for  $\overline{i_{n,in,tot}}$  because the realized circuit contains more poles (second dominant pole is at the output of the voltage amplifier and the other one from the common-collector stage). As expected, noise is dominated by base and collector shot noise of  $T_1$  and  $T_2$  and thermal noise of the base resistances (66% of the total noise). Feedback resistors  $R_F$  contribute to the noise about 22%. Noise percentage of each device is presented in Appendix A. Using the Equation (3.13), sensitivity of the differential TIA at BER of  $10^{-12}$  can be found as  $15 \text{ } \mu\text{A}_{pp}$ . by using the Equation (3.24), averaged input noise current  $\overline{i_{n,in,avg}}$  can be found as  $11.18 \text{ pA}/\sqrt{\text{Hz}}$ . Maximum peak-to-peak input current of the TIA is  $400 \text{ } \mu\text{A}_{pp}$ . Although linearity of the signal is preserved up to  $1 \text{ mA}_{pp}$  input current levels, higher peak-to-peak currents than  $400 \text{ } \mu\text{A}_{pp}$  will cause  $V_{CE}$  of the  $T_1$  and  $T_2$  to exceed collector-emitter junction breakdown voltage.

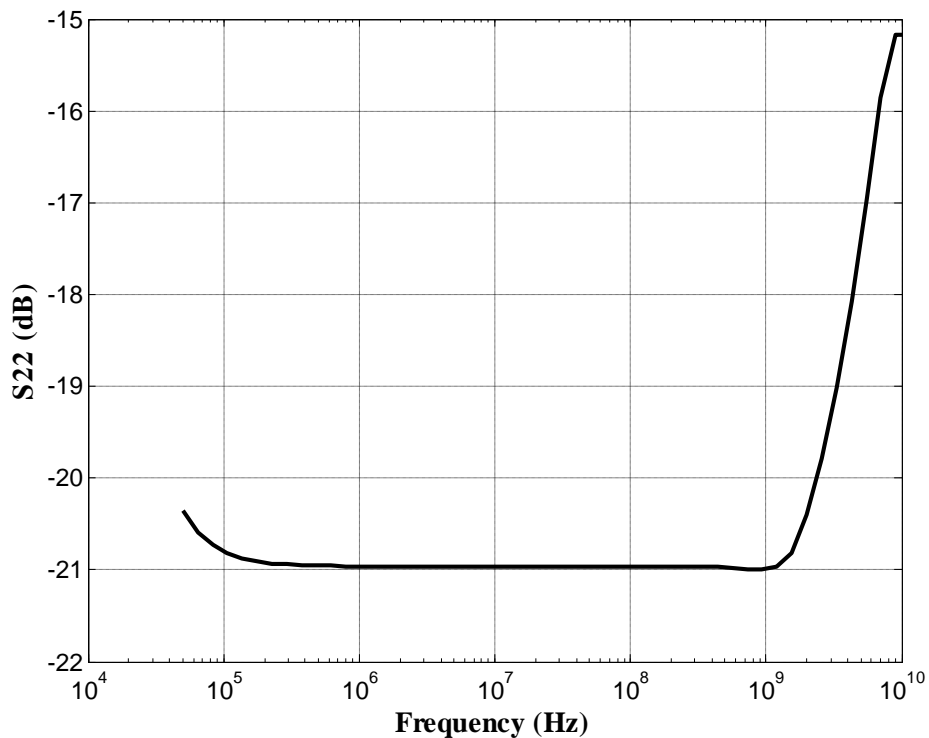
Differential output waveforms of the TIA is depicted in Figure 4.7. The TIA is driven with a NRZ data stream of 10 Gbit/s and  $2^{31}-1$  pseudo random bit sequence (PRBS) with the amplitude of  $15 \text{ } \mu\text{A}_{pp}$  and  $400 \text{ } \mu\text{A}_{pp}$ , respectively. Very good signal shape with little overshoot is obtained. Differential output swing for the first case is  $12 \text{ mV}_{pp}$ . In the second case, maximum differential output swing is  $320 \text{ mV}_{pp}$ .



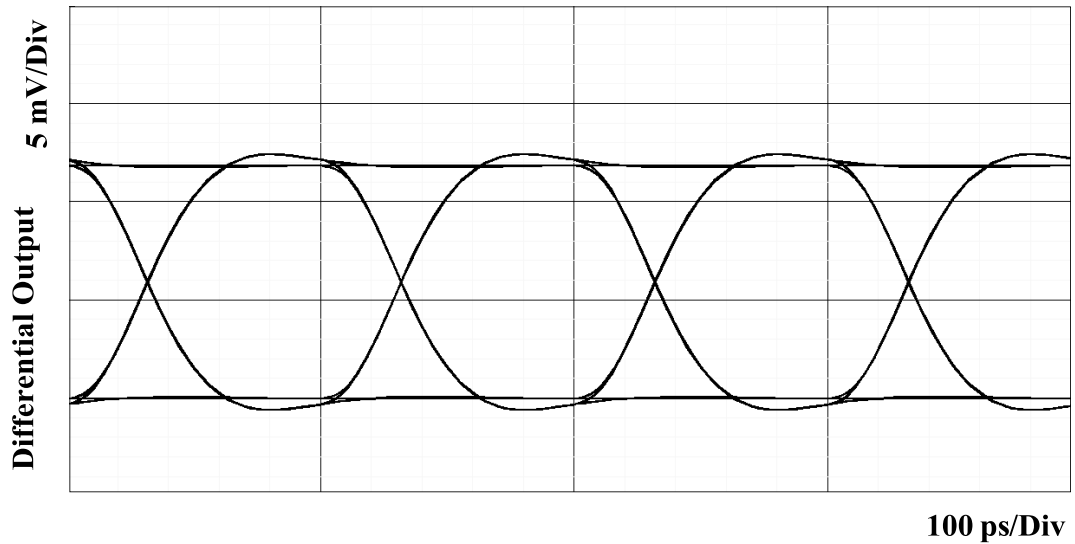
**Figure 4.7:** Differential output waveform of the circuit. The input data stream is NRZ 10 Gbit/s  $2^{31}-1$  PRBS. (a) Input current is  $15 \mu\text{A}_{pp}$ . (b) Input current is  $400 \mu\text{A}_{pp}$ .

Figure 4.8 illustrates single-ended output  $S_{22}$  parameter of the realized circuit. The proposed differential TIA is intended for the integrated receiver comprising both TIA and PA in a single chip. If differential TIA is not implemented in the single die together with the PA, then TIA must have capability to drive  $50\ \Omega$  loads. Hence,  $30\ \Omega$  resistors are placed to the both outputs for impedance matching.  $S_{22}$  is less than  $-15\ \text{dB}$  over the bandwidth implying good matching. Adding matching resistors sacrifices the midband transimpedance gain  $5\ \text{dB}\Omega$  loss per output.

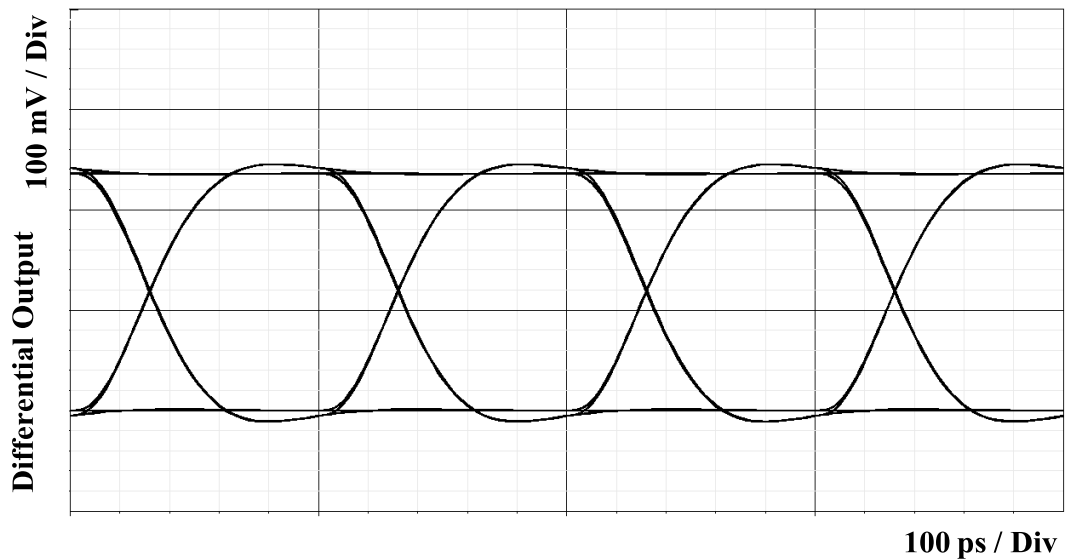
Eye diagrams resulted in a wide eye opening shown in Figure 4.9. The TIA input is fed with two input currents:  $15\ \mu\text{A}_{\text{pp}}$  and  $300\ \mu\text{A}_{\text{pp}}$ . The data stream is again  $10\ \text{Gbit/s}$  and  $2^{31}-1$  PRBS. To demonstrate the eye diagram performance two scenarios are realized: In the first case, outputs are loaded with  $100\ \text{fF}$  capacitors to characterize the effect of the subsequent stage [47]. In the latter,  $30\ \Omega$  matching resistors are added to the both outputs in case TIA has to drive  $50\ \Omega$  transmission line. The eye openings are clear for both horizontal and vertical openings.



**Figure 4.8:** Single-ended  $S_{22}$  parameter of the realized TIA.  $30\ \Omega$  resistors are added to the both output for  $50\ \Omega$  matching.

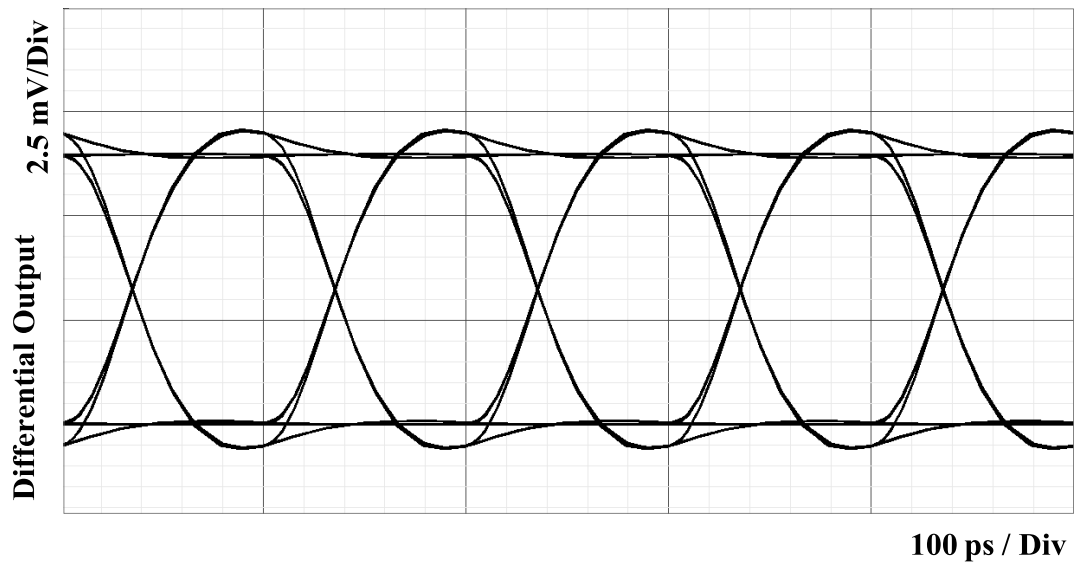


(a)

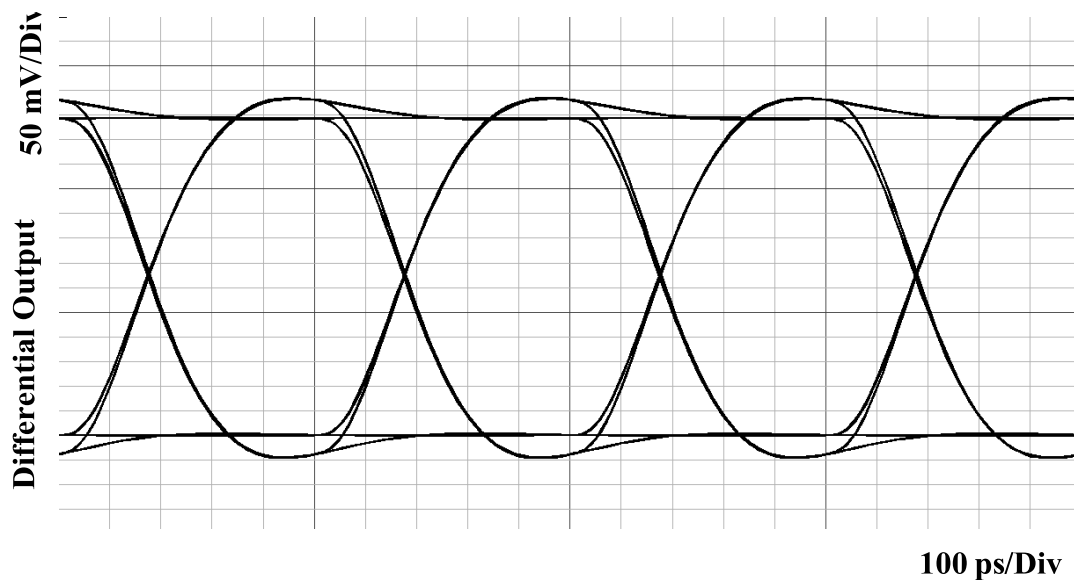


(b)

**Figure 4.9:** Eye diagrams showing differential output at 10 Gbit/s  $2^{31} - 1$  PRBS data stream. (a) Input current is  $15 \mu\text{A}_{pp}$ , both outputs are loaded with 100 fF capacitor. (b) Input current is  $300 \mu\text{A}_{pp}$ , both outputs are loaded with 100 fF capacitor. (c) Input current is  $15 \mu\text{A}_{pp}$ , both outputs are loaded with  $50 \Omega$  resistors. (d) Input current is  $300 \mu\text{A}_{pp}$ , both outputs are loaded with  $50 \Omega$  resistors. In the case of (c) and (d)  $30 \Omega$  matching resistors are added to the both outputs.



(c)



(d)

**Figure 4.9 (continued):** Eye diagrams showing differential output at 10 Gbit/s  $2^{31}$ -1 PRBS data stream. (a) Input current is  $15 \mu\text{A}_{\text{pp}}$ , both outputs are loaded with 100 fF capacitor. (b) Input current is  $300 \mu\text{A}_{\text{pp}}$ , both outputs are loaded with 100 fF capacitor. (c) Input current is  $15 \mu\text{A}_{\text{pp}}$ , both outputs are loaded with  $50 \Omega$  resistors. (d) Input current is  $300 \mu\text{A}_{\text{pp}}$ , both outputs are loaded with  $50 \Omega$  resistors. In the case of (c) and (d)  $30 \Omega$  matching resistors are added to the both outputs.

## 5. CONCLUSION

In this dissertation, the differential SiGe transimpedance amplifier for 10 Gbit/s fiber optical receivers is realized and its results are presented. The TIA is optimized for the best phase linearity over the bandwidth resulted in a group delay variation less than 1 ps. No inductor is used to achieve wideband operation.

The differential structure of the TIA makes it immune to the effect of the supply and substrate noise. Results are appreciable. In addition to flat frequency response, 9 GHz bandwidth is provided. Differential transimpedance gain is almost 58 dB $\Omega$ . The electrical sensitivity of the proposed TIA is 15  $\mu\text{A}_{\text{pp}}$ . Power consumption is 71 mW and maximum differential output swing is 320 mV $_{\text{pp}}$ . The figure-of-merit averaged input-referred-noise current is 11.18 pA/ $\sqrt{\text{Hz}}$ . It has been demonstrated that the differential TIA is well suited for 10 Gbit/s data rate and for OC-192 specifications.

Table 5.1 summarizes simulation performance of the realized circuit and makes comparison to the some existing designs. III-V technologies such as GaAs and InP have recently not preferred in the photoreceivers because they consume much more power for the same speed. In reference [48] and [49], there are no noise and sensitivity results, which are very important for a low-noise front-end preamplifier. CMOS has lower transimpedance for the same speed [50]. In [48], although more than 10 GHz bandwidth is achieved, noise performance is not provided. As widely discussed in this thesis, as the bandwidth of the TIA is increased pointlessly, the noise issue will be a big bottleneck for a transimpedance amplifier.

The first goal when realizing an optical receiver must be to integrate all of the analog and digital blocks in the same package as well as preserving high performance and reducing production expenses.

**Table 5.1:** TIA performance summary and comparison to the some existing works.

References	[48]	[49]	[50]	[This Study]
Technology	0,35 $\mu\text{m}$ SiGe	60 fT GaAs	0,18 $\mu\text{m}$ CMOS	0,35 $\mu\text{m}$ SiGe
Transimpedance	60.49 dB $\Omega$ differential	28 dB $\Omega$ differential	40 dB $\Omega$ differential	57.9 dB $\Omega$ differential
Bandwidth	10.42 GHz	10.5 GHz	8.69 GHz	9 GHz
Group delay variation	-	-	-	<1 ps
Averaged input noise	-	-	96.48 pA/ $\sqrt{\text{Hz}}$	11.18 pA/ $\sqrt{\text{Hz}}$
Sensitivity(@ BER = $10^{-12}$ )	-	-	-	15 $\mu\text{App}$ Electrical
Max. differential output swing	466 mV	-	-	320 mV
Supply voltage	3.3 V	-5.2 V	1.8 V	3.3 V
Power dissipation	148 mW	368 mW	15.33 mW	71 mW
Work	Simulation	Fabricated chip	Simulation	Simulation

## REFERENCES

- [1] **Gao, J.** (2011). *Optoelectronic Integrated Circuit Design and Device Modeling*, *Jon Wiley & Sons Pte Ltd*, Shanghai, China.
- [2] **Agrawal, G. P.** (2010). *Fiber-Optic Communication Systems*, *The Institute of Optics, Jon Wiley & Sons Inc*, University of Rochester, Rochester, New York, USA.
- [3] **Buchwald, A., Martin, K. W.** (1994). *Integrated Fiber-Optic Receivers*, *Kluwer Academic Publishers*, Boston, USA.
- [4] **Suzaki, T., Soda, M., Takenori M., Tezuka, H., Ogawa, C., Fujita, S., Takemura, H., Tashiro, T.** (1992). A Si Bipolar Chip Set for 10Gb/s Optical Receiver, *IEEE 39th Solid-State Circuits Conference*, pp: 100-101.
- [5] **Seng, C. W., Sern, T. Y., Seng, Y. K.** (2013). A low power wideband differential transimpedance amplifier for optical receivers in 0.18  $\mu\text{m}$  CMOS, *IEEE 11th International Conference on New Circuits and Systems (NEWCAS)*, pp: 1-4.
- [6] <<https://learningnetwork.cisco.com/thread/4414>> date retrieved 01.10.2013.
- [7] **Bishnu, P. P.** (2006). *Guided Wave Optical Components and Devices*, *Indian Institute of Technology, Elsevier Academic Press*, Amsterdam, Holland.
- [8] **Dries, J.C., Bush, M.G., Lange, M., Brubaker, R.M., Mykietyn, E., Cohen, M.J., Olsen, G.H.** (2000). Demonstration of a 40 Gb/s, 4 Channel Optical Receiver Array, *IEEE 13th Annual Meeting on Lasers and Electro-Optics Society (LEOS)*, 2000, vol 1, pp: 344-345.
- [9] **Prasad S, Schumacher, H., Gobinath, A.** (2009). *High-Speed Electronic and Optoelectronics*, *Cambridge University Press*, Cambridge, England.
- [10] **Sackinger, E.** (2005). *Broadband circuits for optical fiber communication*. *Wiley-Interscience*. New Jersey, USA.
- [11] **Graeme, J. G.** (1995). *Photodiode Amplifiers*, *McGraw Hill*, Boston, USA.
- [12] **Jung, D.Y., Park, S.H., Lee, K.H., Chang, W.J., Nam, E.S., Lim, J.W., Park, C.S.** (2002). An InGaP/GaAs HBT transimpedance amplifier for 10 Gb/s optical communication. *IEEE 3rd International Conference on Microwave and Millimeter Wave Technology (ICMMT)*, pp: 974-977.
- [13] **Fukuyarna, H., Murata, K., Sano, K., Kitabayashi, H., Yamane, Y., Enoki, T., Sugahara, H.** (2003). Optical receiver module using an InP HEMT transimpedance amplifier for over 40 Gbit/s. *IEEE Gallium Arsenide Integrated Circuit Symposium, 25th Annual Technical Digest*, pp: 237-240.
- [14] **Tang, W., Plant, D. V.** (2006). A low power 3.125Gb/s/Channel parallel optical receiver for very short reach applications. *IEEE 23rd Biennial Symposium on Communications*, pp: 35-38.

- [15] **Li, C., Palermo, S.** (2013). A Low-Power 26-GHz Transformer-Based Regulated Cascode SiGe BiCMOS Transimpedance Amplifier, *IEEE Journal of Solid-State Circuits*, vol: 48, issue 5, pp: 1264-1275.
- [16] **Ramaswami, R., Sivarajan, K. N.** (2002). Optical Networks: A Practical Perspective, *Morgan Kaufmann Publishers*, San Fransisco, USA.
- [17] **Noe, R.** (2010). Essentials of Modern Optical Fiber Communications, *Springer*, Heilderberg, Germany.
- [18] **Nishimoto, H., Okiyama, T., Kuwata, N., Arai, Y., Miyuchi, A. and Touge, T.** (1988). New Method of analyzing eye patterns and its application to high speed optical transmission Systems, *IEEE Journal of Lightwave Technology*, vol:6, issue 5, pp: 678-685.
- [19] **Razavi, B.** (2003). Design of Integrated Circuits for Optical Communications, *McGraw-hill*, Los Angeles, USA.
- [20] **Muller, P., Leblebici, Y.** (2007). CMOS Multichannel Single-Chip Receivers for Multi-Gigabit Optical Data Communications, *Springer*, Eton, Switzerland.
- [21] **Hermans, C., Steyaert, M.** (2007). Broadband Opto-Electrical Receivers in Standard CMOS, *Springer*, Dordrecht, The Netherlands.
- [22] **Maas, S. A.** (2005). Noise in Linear and Nonlinear Circuits, *Artech House*, Boston, USA.
- [23] **Gray, P. R., Hurst, P.J., Lewis, S. H., Meyer, R. G.** (2006). Analaysis and Design of Analog Integrated Circuits, *John Wiley*, New York, USA.
- [24] **Nguyen, D. B., Le, Q., Le, Y., Le. H. and Lee, S.** (2005). A High Linearity, Efficient Bandwidth, and High Stability Transimpedance Amplifier, *48th Midwest Symphosium on Circuits and Systems (MWSCAS)*, vol: 1, pp: 167-170.
- [25] **Schneider, K., Zimmermann, H.** (2006). High Sensitive Optical Receivers, *Springer*, Heilderberg, Germany.
- [26] **Vanisri, T., Toumazou, C.** (1995), Integrated High Frequency Low-Noise Current-Mode Optical Transimpedance Preamplifiers: Theory and Practice, *IEEE Journal of Solid-State Circuits*, vol: 30, issue 6, pp: 677-685.
- [27] **Dorf, R. C., Bishop, R. H.** (1988). Modern Control Systems, *Addison-Wesley*, Boston, MA, USA.
- [28] **Neuhauser, M., Rein, H., Wernz, H.** (1996). Low-Noise, High-Gain Si-Bipolar Preamplifiers for 10 Gb/s Optical-Fiber Links Design and Realization, *IEEE Journal of Solid-State Circuits*, vol: 31, issue 1, pp: 24-29.
- [29] **Kang, S. S., Leblebici, Y.** (1999). CMOS Digital Integrated Circuits, *McGraw Hill*, Boston, USA.
- [30] **Hodges, D. A., Jackson, H. G.** (1988). Analysis and Design of Digital Integrated Circuits, *McGraw Hill*, New York, USA.
- [31] **Jiang, F., Chen , J., Wu, D., Wu J., Jin, Z., Liu, X.** (2012). A wide dynamic range transimpedance amplifier with high gain-bandwidth product for 10 Gb/s optical links, *IEEE International Workshop on Microwave and Millimeterwave Circuits and Systems Technology (MMWCST)*, pp: 1-4.

- [32] **Fields, C.H., Tsen, T., McGuire, C., Yoon, Y., Zehnder, D., Thomas, S., Montes, M., Valles, I., Duvall, J., Hussain, T.** (2010). 110+ GHz Transimpedance Amplifier in InP-HBT Technology for 100 Gbit Ethernet, *IEEE Microwave and Wireless Components Letters*, vol: 20, issue: 8, pp: 465-467.
- [33] **Ohhata, K., Masuda, T., Imai, K., Takeyari, R., Washio, K.** (1999). A wide-dynamic-range, high-transimpedance Bipolar preamplifier IC for 10-Gb/s optical fiber links, *IEEE Journal of Solid-State Circuits*, vol: 34, issue: 1, pp: 18-24.
- [34] **Liu, F.Y., Patil, D., Lexau, J., Amberg, P., Dayringer, M., Gainsley, J., Moghadam, H.F., Zheng, X., Cunningham, J.E., Krishnamoorthy, A.V., Alon, E., Ho, R.** (2012). 10-Gbps, 5.3-mW Optical Transmitter and Receiver Circuits in 40-nm CMOS, *IEEE Journal of Solid-State Circuits*, vol: 47, issue: 9, pp: 2049-2067.
- [35] <[http://www.eng.auburn.edu/~guofu/sige\\_intro.htm](http://www.eng.auburn.edu/~guofu/sige_intro.htm)> date retrieved 03.08.2013.
- [36] **Ashburn, P.** (2003). SiGe Heterojunction Bipolar Transistors, *John Wiley & Sons Ltd*, University of Southampton, Southampton, UK.
- [37] **Cressler, J. D., Niu, G.** (2003). Silicon-Germanium Heterojunction Bipolar Transistors, *Artech House*, Boston, USA.
- [38] **Rieh, S. J.,** (2002). SiGe HBTs with Cut-off Frequency of 350 GHz, *IEEE international on Electron Devices Meeting (IEDM)*, pp.771-774.
- [39] **Kasper, E., and Paul D. J.** (2005). Silicon Quantum Integrated Circuits, *Springer*.
- [40] **Zeghbrock, V. B.,** 2008. Principles of Semiconductor Devices and Heterojunctions, *Prentice Hall*, Boston, USA.
- [41] **Vatannia, S., Yeung, P. and Lu, C.** (2005). A Fast Response 155-Mb/s Burst-Mode Optical Receiver for PON. *IEEE Photonics Technology Letters*, vol: 17, no. 5, pp: 1067-1069.
- [42] **Rieh, J.-S., Qasaimeh, O., Klotzkin, D., Lu, L.-H., Yang, K., Katehi, L.P.B., Bhattacharya, P., Croke, E.T.** (1997). Monolithically Integrated SiGe/Si PIN HBT Front-End Transimpedance Photoreceivers. *IEEE/Cornell Conference on Advanced Concepts in High Speed Semiconductor Devices and Circuits*, Page(s): 322 – 331.
- [43] **Jin, J. D., Hsu, S.,** (2008). A 75-dB $\Omega$  10-Gb/s Transimpedance Amplifier in 0.18- $\mu$ m CMOS Technology, *IEEE Photonics Technology Letters*, vol: 20, issue: 24, pp: 2177 – 2179.
- [44] **Han, L., Yu, M., Zong, L.** (2010). Bandwidth Enhancement for Transimpedance Amplifier in CMOS Process. *IEEE 3rd International Conference on Biomedical Engineering and Informatics (BMEI)*, vol: 7, pp: 2839 – 2842.
- [45] **Kim, H. H., Chandrasekhar, S., Burrus, C. A. and Bauman, J.** (2001). A Si BiCMOS transimpedance amplifier for 10-Gb/s SONET receiver. *IEEE Journal of Solid-State Circuits*, SC 6(5):769-776.
- [46] **EL-Diwany, M. H., Roulston, D. J., Chamberlain S. G.** (1981). Design of low-noise bipolar transimpedance preamplifiers for optical receivers. *IEE Proc. G, Electron. Circ. & Syst.*, 128, pp: 299-305.

- [47] **Samadi, M. R., Karsilayan, A. I. and Silva-Martinez, J.** (2002). Design of Transimpedance and Limiting Amplifiers for 10 Gb/s Optical Communication Systems. *IEEE 45th Midwest Symposium on Circuits and Systems (MWSCAS)*, vol: 3, pp: 164-167.
- [48] **Fenfei H., Jingxing D.** (2008). 0.35  $\mu\text{m}$  SiGe BiCMOS Front-End Amplifier For 10Gb/s Optical Receiver. *IEEE International Conference on Microwave and Millimeter Wave Technology (ICMMT)*, pp: 249 – 252.
- [49] **Zhou L., Wu D., Wu J., Jin Z., and Liu X.** (2012). Design of a 10GHz Bandwidth Variable Gain Amplifier using a GaAs HBT Technology. *IEEE International Workshop on Microwave and Millimeter Wave Circuits and System Technology (MMWCST)*, pp: 1-4.
- [50] **Huang T., Zhang Q., Zhang W.** (2011). A Novel Transimpedance Amplifier for 10 Gbit/s Optical Communication System. *IEEE 9th International Conference on ASIC, ASICON*, pp: 843 – 846.

## **APPENDICES**

**APPENDIX A:** Program Schematic and Relevant Figures.



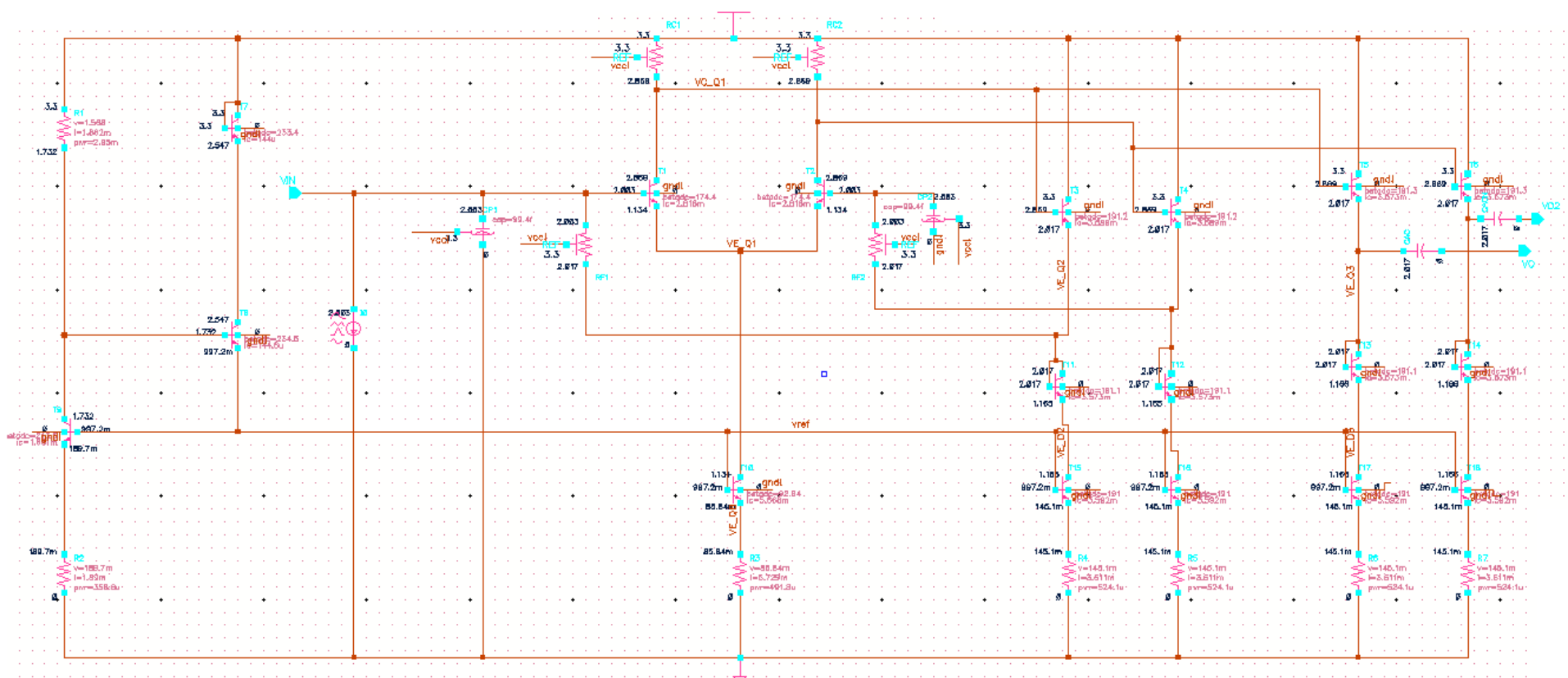


Figure A.1: Program schematic of realized TIA.

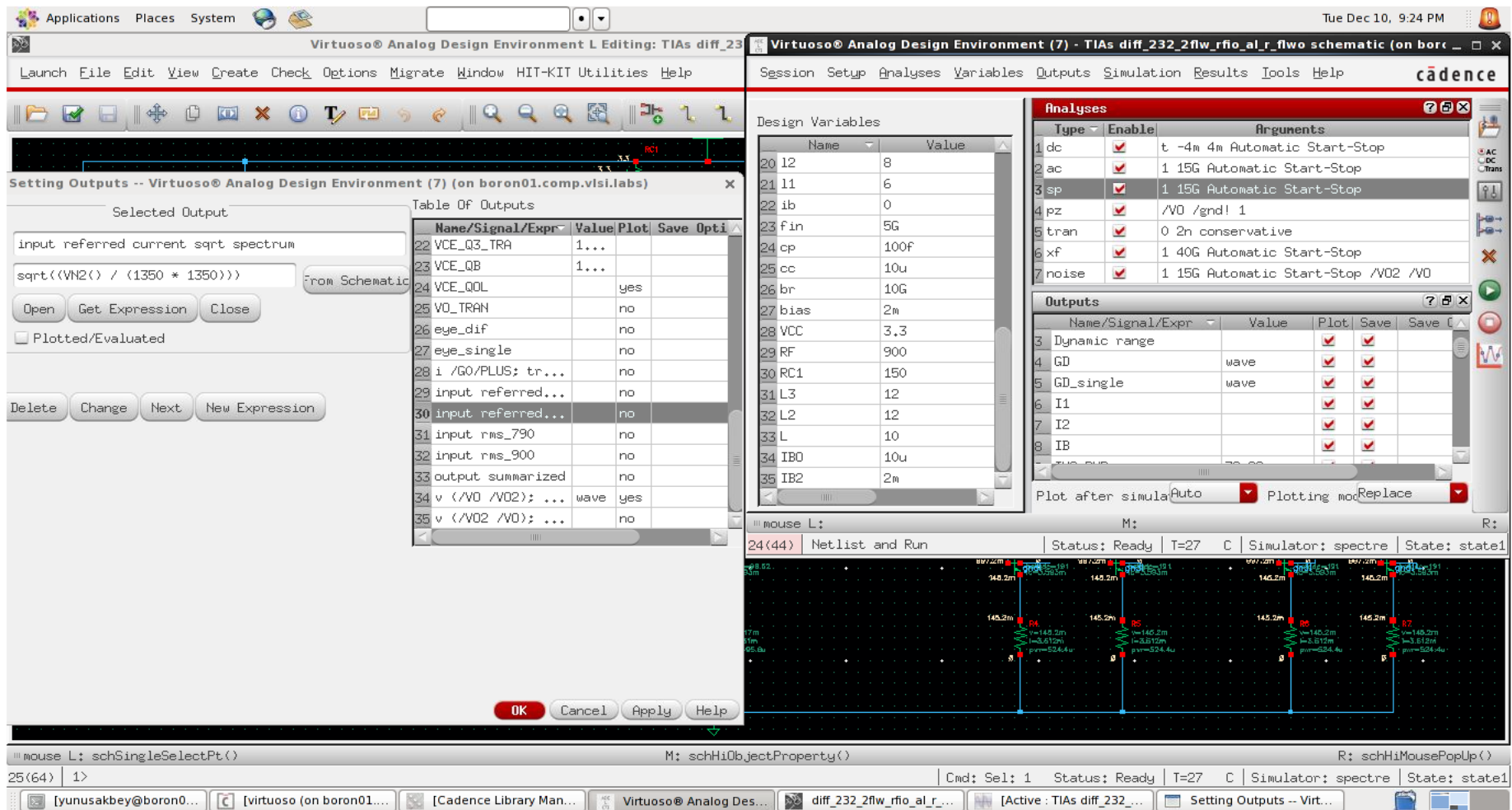


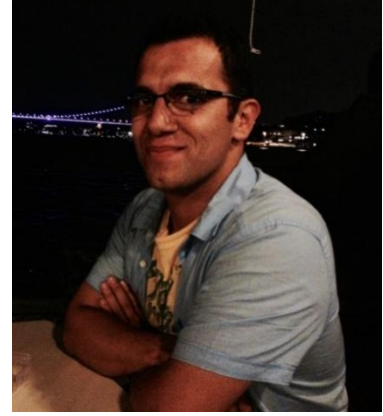
Figure A.2: Simulation and values.

Window Expressions Info					Window Expressions Info				
Device	% Of Total	Inp Ref Noise Param		Noise Contribution					
/Q12	33.04	1.04065e-06	total	0.00054891	/Q21	1.15	1.82917e-07	total	0.000102304
			rbi	0.000399602				rbi	6.8038e-05
			itzf	0.00027534				itzf	6.13488e-05
			ibe	0.000187127				ibe	3.31271e-05
			rbx	0.000149235				rbx	2.46491e-05
			re	8.84115e-05				re	1.68522e-05
			rcx	2.64315e-05				rcx	9.17621e-06
			fn	2.36179e-06				rci	1.69149e-07
			rci	9.3434e-07				fn	1.68413e-07
			ibep	1.5055e-12				ibep	3.36078e-13
			fnp	6.85767e-20	/Q22	1.15	1.82917e-07	total	0.000102304
			iccp	0				rbi	6.8038e-05
/Q11	33.04	1.04065e-06	total	0.00054891				itzf	6.13488e-05
			rbi	0.000399602				ibe	3.31271e-05
			itzf	0.00027534				rbx	2.46491e-05
			ibe	0.000187127				re	1.68522e-05
			rbx	0.000149235				rcx	9.17621e-06
			re	8.84115e-05				rci	1.69149e-07
			rcx	2.64315e-05				fn	1.68413e-07
			fn	2.36179e-06				ibep	3.36078e-13
			rci	9.3434e-07				fnp	6.45369e-21
			ibep	1.5055e-12				iccp	0
			fnp	6.85767e-20	R11.rpoly2rf2	0.95	1.81748e-07	total	9.29358e-05
			iccp	0					9.29358e-05
RF1.rpoly2rf2	5.89	3.6456e-07	total	0.000231763	R12.rpoly2rf2	0.95	1.81748e-07	total	9.29358e-05
				0.000231763					9.29358e-05
RF2.rpoly2rf2	5.89	3.6456e-07	total	0.000231763	/R11	0.95	1.81695e-07	total	9.29163e-05
				0.000231763					9.29163e-05
/RF1	5.06	3.24913e-07	total	0.000214842	/R12	0.95	1.81695e-07	total	9.29163e-05
				0.000214842					9.29163e-05
/RF2	5.06	3.24913e-07	total	0.000214842	/Q31L	0.28	1.13357e-07	total	5.08888e-05
				0.000214842				rbi	3.9934e-05
/Q31	2.12	2.67346e-07	total	0.000139134				itzf	2.2584e-05
			rbi	0.000102059				rbx	1.58602e-05
			itzf	6.95598e-05				ibe	1.08338e-05
			ibe	4.14229e-05				re	9.88482e-06
			rbx	4.07317e-05				rcx	4.27434e-06
			re	2.52506e-05				fn	8.28126e-08
			rcx	9.54726e-06				rci	7.21032e-08
			fn	2.88973e-07				ibep	7.23926e-14
			rci	2.00649e-07				iccp	2.23375e-14
			ibep	3.51867e-13				fnp	2.17012e-21
			fnp	7.52516e-21	/Q32L	0.28	1.13357e-07	total	5.08888e-05
			iccp	0				rbi	3.9934e-05
/Q32	2.12	2.67346e-07	total	0.000139134				itzf	2.2584e-05
				0.000139134				rbx	1.58602e-05

Figure A.3: Noise contribution of each device.



## CURRICULUM VITAE



**Name Surname:** Yunus AKBEY  
**Place and Date of Birth:** İstanbul, 1982  
**Address:** Esenyurt, İstanbul  
**E-Mail:** yakbey@gmail.com  
**B.Sc.:** Department of Avionics, Faculty of Aeronautics and Astronautics, Anadolu University

### Professional Experience:

Yunus Akbey received the B.Sc. degree from the Department of Avionics, at Anadolu University in 2006. His research interests are microwave and RF circuit design, design of analog IC topologies.

### List of Publications Papers:

- Akbey, Y., Palamutçuoğulları, O. (2013). A Broadband, Differential Transimpedance Amplifier in 0.35  $\mu\text{m}$  SiGe BiCMOS Technology for 10 Gbit/s Fiber Optical Front-Ends. *Journal of Analog Integrated Circuits and Signal Processing, Springer*, vol: 74, issue: 1, pp: 155-162.

### List of Conferences Papers:

- Akbey, Y., Palamutcuogulları, O. (2011). 9 GHz Differential SiGe Transimpedance Amplifier for 10 Gbit/s Fiber Optical Front-Ends. *7th International Conference on Electrical and Electronics Engineering (ELECO)*, pp. II-250–II-254.